Electronic Thesis and Dissertation Repository

8-23-2019 3:00 PM

Vegetation and Tree Species Classification Using Multidate and High-resolution Satellite Imagery and Lidar Data

Matthew Roffey
The University of Western Ontario

Supervisor
Wang, Jinfei
The University of Western Ontario

Abstract

Remote sensing can play a key role in understanding the makeup of urban forests. This thesis analyzes how high-resolution multispectral imagery, lidar point clouds, and multidate multispectral imagery allow for improved classification of London, Ontario's urban forest. Chapter 2 uses object-based support vector machine classification (SVM) to classify five types of trees using features derived from Geoeye-1 imagery and lidar data. This results in an overall accuracy of 85.08% when features from both data sources are combined, compared with 77.73% when using only lidar features, and 71.85% when using only imagery features. Chapter 3 makes use of Planetscope and VENuS images from different seasons to classify deciduous trees, conifers, non-tree vegetation, and non-vegetation using SVM. Using multidate Planetscope images increases overall accuracy to 83.11% (8.19 percentage points more than single-date Planetscope classification), while using multidate VENuS images increases accuracy to 72.18% (2.22 percentage points higher than single-date VENuS classification).

Keywords

remote sensing, urban forest, support vector machine, lidar, multitemporal, multispectral

Summary for Lay Audience

Urban trees provide numerous benefits to a city's environment, as well as the health of its people. It is often necessary for urban planners to know the makeup of tree species in the urban forest. Trees can be identified and classified by species using remotely sensed data. This data is often imagery, but other data sources such as lidar (3D point data from laser pulses) also allow for classification. This thesis focuses on two different data sources for classifying trees. The first source is a combination high-resolution imagery and lidar data. The second contains multiple images of the same area on different days of the year.

In chapter 2, features derived from imagery and lidar, which ultimately represent the chemical and structural traits of trees, are used to classify five types of trees in London, Ontario. Object-based classification is used, meaning individual trees crowns are delineated and classified, rather than just classifying individual pixels. It is found that lidar features perform better than imagery features, resulting in more trees being classified accurately. However, combining features from both data sources results in an even higher level of accuracy.

Chapter 3 focuses on using imagery obtained on different dates, to capture seasonal changes in vegetation. Four dates are used, representing different stages of leaf development in trees. Two sensors are used, Planetscope and VENuS, which have rarely been used for multidate tree classification. Planetscope has higher-resolution, but has fewer bands, meaning it captures less detailed spectral information. VENuS has more bands but lower spatial resolution. Classification is performed on image pixels and classifies the study area into deciduous trees, conifers, non-tree vegetation and non-vegetation. Significant improvement to accuracy is found for Planetscope when using multiple dates, in particular using images from April when leaves are not present and July when leaves are fully grown. Improvement from using multiple dates is smaller when using VENuS.

Acknowledgments

Table of Contents

List of Tables

List of Figures

List of Appendices

Chapter 1

1   Introduction

1.1   Importance of Urban Trees

From isolated trees along city streets to dense stands within parks, the urban forest is a prominent aspect of many cities. The urban forest refers to all woody vegetation within and around human settlements (Miller 1997). This includes individual trees on streets and in yards, woodlands of naturally growing trees, as well as plantations (Konijnendijk 2005). Urban forests provide numerous benefits to both the environment and the human population of cities. As they come from the natural functioning of an ecosystem, these benefits can be defined as ecosystem services (Carreiro, Song, and Wu 2008).

Ecosystem services include improvements to air quality, temperature, biodiversity, and human physical and mental health. Trees benefit air quality by removing pollutants and particulates which are trapped on the surface of the tree and absorbed into it (Carreiro, Song, and Wu 2008). Trees can also help reduce temperatures, which is a major concern due to urban heat effects. For example, parks are often 2-3 °C cooler than the surrounding city (Konijnendijk 2005). Shading also reduces the temperature of buildings, therefore lowering cooling costs and energy use, while trees acting as wind buffers can reduce heating costs in winter (Carreiro, Song, and Wu 2008). From a broader climatic perspective, trees are also beneficial as they sequester carbon during their lifetimes, reducing the greenhouse effect (Carreiro, Song, and Wu 2008). Trees also improve biodiversity by providing habitat for other species. This is most significant with old, primary forest, but even individual trees provide habitat for birds and invertebrates (Konijnendijk 2005). There are also direct health benefits for humans. Access to urban forests can improve people's physical health by encouraging them to go outside and be active. Even mental health may be improved, as trees have been tied to stress reduction (Konijnendijk 2005).

Not all trees provide these benefits equally. For example, a study of trees' ability to trap particulates found differences based on size and species. Other trees may be unsuited to reducing pollution due to their intolerance to certain pollutants (Dawe 2011). In a park, the type of trees selected and their placement (e.g. individual trees or clusters of trees) will affect how people use the area around them (Konijnendijk 2005). The conditions that trees face also must be considered. Street trees will face more difficulties, such as polluted road runoff and higher wind stress, compared to trees in a denser wooded area (Konijnendijk 2005). A diverse range of species is also important in order to minimize the impacts of pests or diseases that may target only a certain type of tree (Carreiro, Song, and Wu 2008). Tree biodiversity can also be considered an ecosystem service in its own right (Alvey 2006). Urban forests are often the location where non-native species are introduced and spread, but they also have the potential for high biodiversity (Alvey 2006). This is reflected within Ontario, with a number of cities in Southern Ontario establishing plans that support increasing the number of native tree species (Almas and Conway 2016).

1.2   Tree Classification Using Remote Sensing

Due to the benefits provided by trees, and the variations in these benefits between species, it is necessary to have knowledge of tree species composition. It is one of the key components of urban tree inventories, along with factors such as determining tree size and condition (Miller 1997). Remote sensing can assist in obtaining this information. Older methods included making use of manual interpretation of aerial images to determine tree composition (Miller 1997). Now, a wide variety of data sources can be used as input for algorithms that are capable of classifying trees.

Remote sensing tree classification most commonly uses imagery (Fassnacht et al. 2016). Imagery is gathered by passive remote sensors, which measure electro-magnetic energy reflected of off objects in the area the sensor is monitoring. The sensor itself does not emit energy. The sensor typically contains multiple bands, which sense electro-magnetic energy from certain wavelength ranges. The number of bands differs between sensors. A sensor with more than 50 bands is defined as hyperspectral, more than 10 as superspectral and less than 10 (but still with multiple bands) as multispectral (Jones and

Vaughan 2010). A larger number of bands means that a difference that exists only in a small wavelength range may be detected by hyperspectral, but not with lower spectral resolution sensors. Vegetation, including trees, typically have similar reflectance patterns: low reflectance in blue and red wavelengths, somewhat higher reflectance in green wavelength and much higher reflectance in near infrared wavelengths. Due to the similarities in reflectance, it is sometimes stated that hyperspectral is needed to successfully differentiate vegetation (Alonzo, Bookhagen, and Roberts 2014). In recent years, studies classifying tree species using hyperspectral have become the most common (Fassnacht et al. 2016). However, there are still studies that achieve success using multispectral sensors, albeit typically with lower numbers of classified species (Table 1.1).

Table 1.1: Past remote sensing studies on tree classification

Year/Author	Sensor	# Bands	Resolution (m)	Object/ Pixel	Classes
1998 Martin	AVIRIS	224	20	Pixel	11 (Stands of species, mixed)
2003 Goodenough	Hyperion	242	25	Pixel	10 (Species dominant, other landcover)
2003 Goodenough cont.	Landsat-7	6	25	Pixel	10 (Species dominant, other landcover)
2004 Xiao	AVIRIS	224	3.5	Pixel	16 (Species)
2010 Jones	AISA Dual	492	2	Pixel	11 (Species)
2012 Cho	CAO Alpha	288	1.12	Pixel	6 (Species)
2012 Cho cont.	WorldView 2	8	1.12	Pixel	6 (Species)
2012 Cho cont.	Quickbird	4	1.12	Pixel	6 (Species)
2012 Dalponte	AISA Eagle	126	1	Pixel	8 (Species, other broadleaf, conifer, non-forest)
2012 Immitzer	WorldView 2	8	2	Object	10 (Species)
2012 Jensen	AISA	248	2.2	Object	10 (Species, Genus)
2012 Zhang	AISA Dual	492	1.6	Object	40 (Species)
2013 Adelabu	RapidEye	4	5	Pixel	5 (Species)
2013 Alonzo	AVIRIS	224	3.7	Object	15 (Species)
2014 Alonzo	AVIRIS	224	3.7	Object	29 (Species)
2016 Immitzer	Sentinel-2	13	10	Object	7 (Stands of species)
2017 Liu	CASI 1500	72	1	Object	15 (Species)
2017 Shen	AISA Eagle	64	0.6	Object	5 (Species)

Spatial resolution is another major aspect of a passive sensor. Sensors have different sized instantaneous fields of view, which is the angle in which energy is focused on the sensor. The ground-projected area of the instantaneous field of view determines the spatial resolution. In digital images, this will be the size of one pixel (Jensen 2005). A pixel will have values for each band, representing the measured energy for that area. All objects in that area will influence the value of the pixel. This leads to mixed pixels, in which a pixel represents multiple objects (e.g. multiple trees, tree and surrounding ground

cover). The size of the pixel can determine whether it is possible to separate individual trees. If the pixel size is too coarse to do so, classification may instead be based on pure stands of a single tree species, or mixtures of multiple tree species (Fassnacht et al. 2014). In contrast, higher resolution sensors allow for the classification of individual trees by species, whether for objects or for individual pixels.

In addition to passive sensors, there are also active sensors which emit their own energy and measure its return. Examples include radar and lidar, of which lidar is more commonly used for classifying tree species (Fabian Ewald Fassnacht et al. 2016). Lidar emits laser pulses which are reflected off objects they hit, returning information about the elevation of the object, as well as the amount of returned energy. Further values can be derived from lidar, including numerous measures of tree structure. Lidar can be used on its own to classify tree species or be combined with imagery (Table 1.2).

Table 1.2: Past tree classification studies making use of lidar data

Year/Author	# Classes	Combined with Imagery
2008 Holmgren	3	Yes
2009 Orka	2	No
2010 Korpela	3	No
2012 Dalponte	7	Yes
2012 Vaughn	5	No
2013 Li	4	No
2014 Alonzo	29	Yes
2017 Liu	15	Yes
2017 Shen	5	Yes

Classification algorithms assign classes either to individual pixels (pixel-based classification) or to objects covering multiple pixels (object-based classification). Classification can either be supervised, where image pixels/objects are compared to user-defined training areas, or unsupervised where the classifier automatically selects natural grouping within the image as classes. At the simplest level, classification is based on pixel values, with pixels/objects being assigned to the training class whose spectral values are closest to their own. (Jensen 2005). However, many different classification methods exist which have more complicated means of classification. Commonly used

parametric classifiers, which have assumptions that must be met about the distribution of data, include maximum likelihood classifier and linear discriminant analysis. However, it is becoming more common to use non-parametric methods which do not require assumptions about data distribution (Plaza et al. 2017). Two commonly used methods are support vector machine and random forest (Table 1.3). This thesis focuses on support vector machine classification.

Table 1.3: Classification methods used in previous studies

Year/Author	Classifier
1998 Martin	Maximum Likelihood
2003 Goodenough	Maximum Likelihood
2004 Xiao	Linear Spectral Mixture Analysis
2010 Jones	Support Vector Machine
2012 Cho	Maximum Likelihood
2012 Dalponte	Support Vector Machine, Random Forest
2012 Immitzer	Random Forest, Linear Discriminant Analysis
2012 Jensen	Linear Discriminant Analysis
2012 Zhang	Neuro-fuzzy
2013 Adelabu	Support Vector Machine, Random Forest
2013 Alonzo	Linear Discriminant Analysis
2014 Alonzo	Linear Discriminant Analysis
2014 Ghosh	Support Vector Machine, Random Forest
2016 Immitzer	Random Forest
2017 Liu	Random Forest
2017 Shen	Random Forest

Typically, numerous features are used for classification. The most basic feature is reflectance or pixel values from imagery. For trees, these values (and thus the light reflected off of trees) in related to chemical properties of leaves, the shape and structure of leaves and the shape and structure of the tree canopy (Fassnacht et al. 2016). Many additional classification features can be derived from image pixel values. From lidar, the height and reflected energy of laser points reflected off of trees can be used to derived numerous structural measures. This will be described in more detail in the following chapters.

1.3   Study Area and Data

This thesis focused on the urban forest of London, Ontario. As of the 2016 census, London had a population of 383,437 and an area of 232.48 km^2 (Statistics Canada 2017). The urban forest of London is diverse, with trees in different settings including individual trees along streets, and natural forest in environmentally significant areas. London is also diverse in terms of species. The city is located in the Carolinian zone of Canada, the only primarily deciduous forest in the country. Many species found here are more common in the United States, and not present elsewhere in Canada (Almas and Conway 2016). Additionally, the inventory of city-maintained trees in London makes it clear that many introduced species are present.

The data used to classify the urban forest of London comes from several different sensors. Chapter 2 makes use of high-resolution multispectral Geoeye-1 imagery, as well as lidar data. Chapter 3 uses multispectral Planetscope imagery, and superspectral VENuS imagery, both of which have high spatial resolution, though lower than Geoeye-1. The extents of the study areas of both chapters are shown in the map below (Figure 1.1).
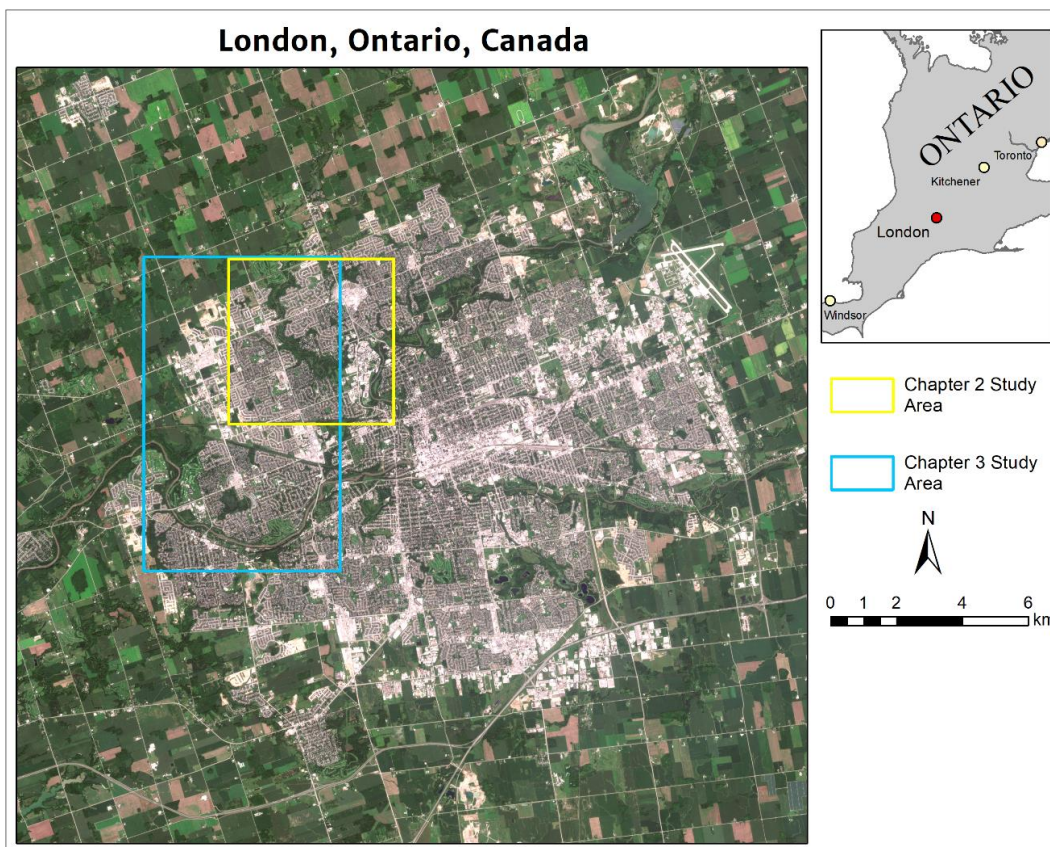
Figure 1.1: Study area for chapters 2 and 3 within London, Ontario. Sentinel-2 image used for city overview.

1.4 Research Objectives

This thesis focuses on further examining the potential of remote sensing for tree classification. Although both methods draw on high resolution multispectral imagery, the exact circumstances vary. Chapter 2 focuses on higher quality, but less accessible data. Namely, Geoeye-1 imagery with 1.6 m resolution is used, alongside lidar data. Both datasets are capable of classifying individual trees at the species level. However, they are not easily obtained. Geoeye-1 is expensive, as are other sensors with similar spatial resolution. The lidar data is from an Ontario government initiative and is publicly available, but repeated coverage of the same area on different dates is not available. In contrast, chapter 3 focuses on imagery with somewhat lower resolution (3 m and 5 m for Planetscope and VENuS respectively). This is still quite high but is too coarse to resolve

most individual trees. These sensors instead benefit from repeated observations of the same area, allowing images from multiple seasons to be used for classification. The research goals of this thesis are mostly focused on specific chapters. The goals of chapter 2 are:

1) Identify which features from high-resolution multispectral imagery and lidar data contribute most to accurately classifying tree species.

2) Determine if combining high-resolution multispectral imagery and lidar results in a higher classification accuracy than either data source can achieve individually.

The goals for chapter 3 are:

3) Assess the ability of multitemporal classification using Planetscope and VENuS to improve the classification of vegetation.

4) Identify which image dates and combinations of dates are best suited to distinguishing vegetation classes.

Chapter 2 involves classifying five different types of trees at the object level, while making use of classification features from high-resolution imagery and lidar data. This combination is common in past research and in general results in a more accurate classification than either source of data can provide on its own. The main purpose of the study is to examine features from imagery and lidar in more detail, testing features that have been used in past studies but rarely all used at one time. In some cases, more variations have been used, such as generating texture measures for all spectral bands rather than only certain bands.

Chapter 3 focuses on multitemporal classification, using multiple images from the same sensor of the same area at different times of the year for classification. This has been tested for various sensors in the past, with accuracy typically higher for classification using multiple image dates. However, the sensors used in this chapter, Planetscope and VENuS, are fairly new and have not yet been used for tree classification using multidate imagery.

1.5   Thesis Organization

This thesis uses integrated article format. Chapter 1 provides background information on the urban forest and tree classification using remote sensing and presents the research objectives. Chapter 2 examines object-based tree species classification using both high-resolution multispectral imagery and lidar data. Chapter 3 details pixel-based multitemporal classification of landcover, including two types of trees (deciduous and coniferous). Chapter 4 summarizes the findings of chapters 2 and 3.

1.6   References

Adelabu, Samuel, Onisimo Mutanga, Elhadi Adam, and Moses Azong Cho. 2013. "Exploiting Machine Learning Algorithms for Tree Species Classification in a Semiarid Woodland Using RapidEye Image." Journal of Applied Remote Sensing 7 (1): 073480. doi:10.1117/1.JRS.7.073480.

Almas, Andrew D., and Tenley M. Conway. 2016. "The Role of Native Species in Urban Forest Planning and Practice: A Case Study of Carolinian Canada." Urban Forestry and Urban Greening 17. Elsevier GmbH.: 54–62. doi:10.1016/j.ufug.2016.01.015.

Alonzo, Michael, Bodo Bookhagen, and Dar A. Roberts. 2014. "Urban Tree Species Mapping Using Hyperspectral and Lidar Data Fusion." Remote Sensing of Environment 148. Elsevier Inc.: 70–83. doi:10.1016/j.rse.2014.03.018.

Alonzo, Mike, Keely Roth, and Dar Roberts. 2013. "Identifying Santa Barbara's Urban Tree Species from AVIRIS Imagery Using Canonical Discriminant Analysis." Remote Sensing Letters 4 (5): 513–521. doi:10.1080/2150704X.2013.764027.

Alvey, Alexis A. 2006. "Promoting and Preserving Biodiversity in the Urban Forest." Urban Forestry and Urban Greening 5 (4): 195–201. doi:10.1016/j.ufug.2006.09.003.

Carreiro, Margaret, Yong-Chang Song, and Jianguo Wu. 2008. Ecology, Planning, and Management of Urban Forests. Springer.

Cho, Moses Azong, Renaud Mathieu, Gregory P. Asner, Laven Naidoo, Jan van Aardt, Abel Ramoelo, Pravesh Debba, et al. 2012. "Mapping Tree Species Composition in South African Savannas Using an Integrated Airborne Spectral and LiDAR System." Remote Sensing of Environment 125. Elsevier Inc.: 214–226. doi:10.1016/j.rse.2012.07.010.

Dalponte, Michele, Lorenzo Bruzzone, and Damiano Gianelle. 2012. "Tree Species Classification in the Southern Alps Based on the Fusion of Very High Geometrical Resolution Multispectral/Hyperspectral Images and LiDAR Data." Remote Sensing of Environment 123. Elsevier Inc.: 258–270. doi:10.1016/j.rse.2012.03.013.

Dawe, Gerald. 2011. The Routledge Handbook of Urban Ecology. Edited by Ian Douglas, David Goode, Michael Houck, and Rusong Wang. New York: Routledge.

Fassnacht, Fabian E., Carsten Neumann, Michael Forster, Henning Buddenbaum, Aniruddha Ghosh, Anne Clasen, Pawan Kumar Joshi, and Barbara Koch. 2014. "Comparison of Feature Reduction Algorithms for Classifying Tree Species with Hyperspectral Data on Three Central European Test Sites." IEEE Journal of Selected Topics in Applied Earth Observations and Remote Sensing 7 (6): 2547–2561. doi:10.1109/JSTARS.2014.2329390.

Fassnacht, Fabian Ewald, Hooman Latifi, Krzysztof Stereńczak, Aneta Modzelewska, Michael Lefsky, Lars T. Waser, Christoph Straub, and Aniruddha Ghosh. 2016. "Review of Studies on Tree Species Classification from Remotely Sensed Data." Remote Sensing of Environment 186: 64–87. doi:10.1016/j.rse.2016.08.013.

Ghosh, Aniruddha, Fabian Ewald Fassnacht, P. K. Joshi, and Barbara Kochb. 2014. "A Framework for Mapping Tree Species Combining Hyperspectral and LiDAR Data: Role of Selected Classifiers and Sensor across Three Spatial Scales." International Journal of Applied Earth Observation and Geoinformation 26 (1). Elsevier B.V.: 49–63. doi:10.1016/j.jag.2013.05.017.

Goodenough, David G., Andrew Dyk, K. Olaf Niemann, Jay S. Pearlman, Hao Chen, Tian Han, Matthew Murdoch, and Chris West. 2003. "Processing Hyperion and ALI for Forest Classification." IEEE Transactions on Geoscience and Remote Sensing 41 (6 PART I): 1321–1331. doi:10.1109/TGRS.2003.813214.

Holmgren, J., Å Persson, and U. Söderman. 2008. "Species Identification of Individual Trees by Combining High Resolution LiDAR Data with Multi-Spectral Images." International Journal of Remote Sensing 29 (5): 1537–1552. doi:10.1080/01431160701736471.

Immitzer, Markus, Francesco Vuolo, and Clement Atzberger. 2016. "First Experience with Sentinel-2 Data for Crop and Tree Species Classifications in Central Europe." Remote Sensing 8 (3). doi:10.3390/rs8030166.

Jensen, John. 2005. Introductory Digital Image Processing: A Remote Sensing Perspective. 3rd ed. Upper Saddle River, N.J.: Pearson Prentice Hall.

Jensen, Ryan R., Perry J. Hardin, and Andrew J. Hardin. 2012. "Classification of Urban Tree Species Using Hyperspectral Imagery." Geocarto International 27 (5): 443–458. doi:10.1080/10106049.2011.638989.

Jones, Hamlyn, and Robin Vaughan. 2010. Remote Sensing of Vegetation: Principles, Techniques, and Applications. Oxford: Oxford University Press.

Jones, Trevor G., Nicholas C. Coops, and Tara Sharma. 2010. "Assessing the Utility of Airborne Hyperspectral and LiDAR Data for Species Distribution Mapping in the Coastal Pacific Northwest, Canada." Remote Sensing of Environment 114 (12). Elsevier Inc.: 2841–2852. doi:10.1016/j.rse.2010.07.002.

Konijnendijk, Cecil C. 2005. Urban Forests and Trees. Edited by Cecil Konijnendijk, Kjell Nilsson, Thomas Randrup, and Jasper Schipperijn. Urban Forests and Trees. Berlin, Heidelberg: Springer Berlin Heidelberg. doi:10.1007/3-540-27684-X.

Korpela, Ilkka, Hans Ole Ørka, Matti Maltamo, Timo Tokola, and Juha Hyyppä. 2010. "Tree Species Classification Using Airborne LiDAR - Effects of Stand and Tree

Parameters, Downsizing of Training Set, Intensity Normalization, and Sensor Type." Silva Fennica 44 (2): 319–339. doi:10.14214/sf.156.

Li, Jili, Baoxin Hu, and Thomas L. Noland. 2013. "Classification of Tree Species Based on Structural Features Derived from High Density LiDAR Data." Agricultural and Forest Meteorology 171–172. Elsevier B.V.: 104–114. doi:10.1016/j.agrformet.2012.11.012.

Liu, Luxia, Nicholas C. Coops, Neal W. Aven, and Yong Pang. 2017. "Mapping Urban Tree Species Using Integrated Airborne Hyperspectral and LiDAR Remote Sensing Data." Remote Sensing of Environment 200 (July). Elsevier: 170–182. doi:10.1016/j.rse.2017.08.010.

Martin, M.E, S.D Newman, J.D Aber, and R.G Congalton. 1998. "Determining Forest Species Composition Using High Spectral Resolution Remote Sensing Data." Remote Sensing of Environment 65 (3): 249–254. doi:10.1016/S0034-4257(98)00035-2.

Miller, Robert. 1997. Urban Forestry: Planning and Managing Urban Greenspaces. Upper Sadle River, N.J.: Prentice-Hall.

Ørka, Hans Ole, Erik Næsset, and Ole Martin Bollandsås. 2009. "Classifying Species of Individual Trees by Intensity and Structure Features Derived from Airborne Laser Scanner Data." Remote Sensing of Environment 113 (6). Elsevier Inc.: 1163–1174. doi:10.1016/j.rse.2009.02.002.

Plaza, Antonio J, Pedram Ghamisi, Javier Plaza, Yushi Chen, and Jun Li. 2017. "Advanced Spectral Classifiers for Hyperspectral Images: A Review." IEEE Geoscience and Remote Sensing Magazine 5 (1): 8–32. doi:10.1109/mgrs.2016.2616418.

Shen, Xin, and Lin Cao. 2017. "Tree-Species Classification in Subtropical Forests Using Airborne Hyperspectral and LiDAR Data." Remote Sensing 9 (11). doi:10.3390/rs9111180.

Statistics Canada. 2017. London [Population centre], Ontario and Ontario [Province] (table). Census Profile. 2016 Census. Statistics Canada Catalogue no. 98-316-X2016001. Ottawa. Released November 29, 2017.

https://www12.statcan.gc.ca/census-recensement/2016/dp-pd/prof/index.cfm?Lang=E

Vaughn, Nicholas R., L. Monika Moskal, and Eric C. Turnblom. 2012. "Tree Species Detection Accuracies Using Discrete Point Lidar and Airborne Waveform Lidar." Remote Sensing 4 (2): 377–403. doi:10.3390/rs4020377.

Xiao, Q., S. L. Ustin, and E. G. McPherson. 2004. "Using AVIRIS Data and Multiple-Masking Techniques to Map Urban Forest Tree Species." International Journal of Remote Sensing 25 (24): 5637–5654. doi:10.1080/01431160412331291224.

Zhang, Caiyun, and Fang Qiu. 2012. "Mapping Individual Tree Species in an Urban Forest Using Airborne Lidar Data and Hyperspectral Imagery." Photogrammetric Engineering & Remote Sensing 78 (10): 1079–1087. doi:10.14358/PERS.78.10.1079.

Chapter 2

2 Tree Species Classification Using High-resolution Multispectral Imagery and Lidar

2.1 Introduction

2.1.1 Tree Classification Data Sources

Urban trees provide numerous benefits to cities. These include social benefits such as improving the aesthetic appeal of cities, as well as physical benefits like controlling urban heat and air pollution (Konijnendijk 2005). However, many trees within cities are introduced species, which may not aid the proper functioning of the local ecosystem. Increasing the proportion of native tree species within cities is already a target for certain municipalities in Southern Ontario (Almas and Conway 2016). Assessing tree species diversity is also a common goal of tree inventories carried out by cities. However, conducting inventories is expensive and time consuming (Östberg et al. 2013). Identifying species using remote sensing can provide a solution, as it is faster than ground surveys, and potentially more cost effective (Fassnacht et al. 2016).

Both spectral imagery and lidar data have been used to successfully identify tree species. Spectral imagery differentiates tree species on the basis on reflectance differences between species, which are influenced by chemical properties as well as leaf morphology and canopy structure (Fassnacht et al. 2016). Due to the similarity in reflectance between species, this is often performed using hyperspectral sensors (Alonzo, Bookhagen, and Roberts 2014). Hyperspectral sensors measure reflected light using a large number of bands measuring narrow wavelength ranges. In contrast, multispectral sensors measure light using a small number of bands covering large wavelength ranges. However, a number of studies have used multispectral sensors and achieved some success when classifying trees (Goodenough et al. 2003, Immitzer, Atzberger, and Koukal 2012, Adelabu et al. 2013). Cho et al. 2012 found that hyperspectral and four-band Quickbird imagery achieved almost identical overall accuracy.

Lidar functions by emitting laser pulses, which are reflected back to the sensor from objects. Returned lidar pulses contain information on elevation and returned energy. Numerous lidar features can be created from this information, but ultimately they represent the structure of the crown and foliage (Fassnacht et al. 2016). Intensity, representing reflected energy from the laser (often infrared), is associated both with leaf reflectance and structure (Korpela et al. 2010). Lidar data is also capable of tree classification, although studies using solely lidar data generally identify only a few key species (Ørka, Næsset, and Bollandsås 2009, Korpela et al. 2010, Vaughn, Moskal, and Turnblom 2012, Shi et al. 2018).

The combination of spectral and lidar data can better classify tree species than either data source can individually. Increases in overall accuracy when comparing classification using hyperspectral data alone to classification using hyperspectral and lidar data include Dalponte et al. 2012 (6 species and non-forest, 74.1% to 84%), Alonzo et al. 2014 (29 species, 79.2% to 83.4%) and Shen 2017 (5 classes, 88.8% to 90.6%). An especially large increase was Liu 2017 with an increase from 51.1% to 70% with 15 species. The large increase was attributed to the early stage of leaf growth making lidar more useful than spectral data (Liu et al. 2017). Similar improvements were found in studies using multispectral images and lidar such as Holmgren et al. 2008 (3 classes, 84% to 94%) and Ke et al. 2010 (5 species dominant stand classes, 84 kappa to 92 kappa).

2.1.2 Classification Features

Classification features derived from spectral images most commonly include the pixel values or reflectance of the sensor's bands. For object based classification, the mean of the pixels in tree crowns is often used (Fassnacht et al. 2016). Limiting the calculation of the mean to the brightest pixels in the crown has been found to improve accuracy (Shen and Cao 2017). Alternatively, a single pixel from the top of the tree crown may be selected (Zhang and Qiu 2012).

Lidar features generally represent crown density, shape, and surface texture, as well as return intensity (Vaughn, Moskal, and Turnblom 2012). Features based on the height of lidar points include exact heights of points (e.g. maximum height), statistics

calculated from those heights (e.g. mean, skew and kurtosis of height), and percentiles (e.g. height which 95% of lidar points in crown fall below).

The utility of height features varies between studies. Ørka et al. 2009, Vaughn et al. 2012 and Korpela et al. 2010 all found intensity measures to be more useful than height measures. In contrast, Ke et al. 2010 found height useful when classifying natural forest, and Cho et al. 2012 found a 5.8 percentage point increase in overall accuracy when using maximum height alongside spectral data to classify savannah trees.

Image texture refers to the image being rough or smooth. In digital images, it is based on the differences between pixel values (Hall-Beyer 2018). The inclusion of texture improves image classification (Coburn and Roberts 2004). Texture measures can be derived from either the spectral image or a lidar product such as a normalized digital surface model (nDSM). Common measures used include grey level co-occurrence matrix textures (GLCM) which are based on different grey-level combinations within a moving window (Hall-Beyer 2018). Their usefulness varies, with Li et al. 2015 finding them less useful than spectral features, while in Heinzel et al. 2012 GLCM measures from both imagery and nDSM were among the 14 most important features in the study.

2.1.3   Research Objectives

The purpose of this study was to better understand the ability of imagery and lidar to classify tree species. This was accomplished by making use of numerous classification features derived from both high-resolution multispectral imagery and lidar. These included spectral means, texture measures of imagery and a normalized digital surface model, and measures of lidar height and intensity. The overall goals of the study were:

1) Achieve an accurate classification of five types of trees in London, Ontario using support vector machine classification with features derived from high-resolution multispectral Geoeye-1 imagery and lidar.

2) Identify which classification features contribute most to the accuracy of the classification result.

3) Verify if combining high-resolution multispectral imagery and lidar results in a higher classification accuracy than either data source can achieve individually.

2.2 Methodology

2.2.1 Study Area and Data Description

London, Ontario is located in southern Ontario, Canada. The city contains isolated urban trees along streets and on private property, as well as denser clusters of trees within parks and environmentally significant areas. The study area covers approximately 25 km^2 in the north of London, corresponding to the boundary of the study's Geoeye-1 image. This area contains both new and old neighbourhoods, leading to a variety of tree ages and sizes (Figure 2.1)
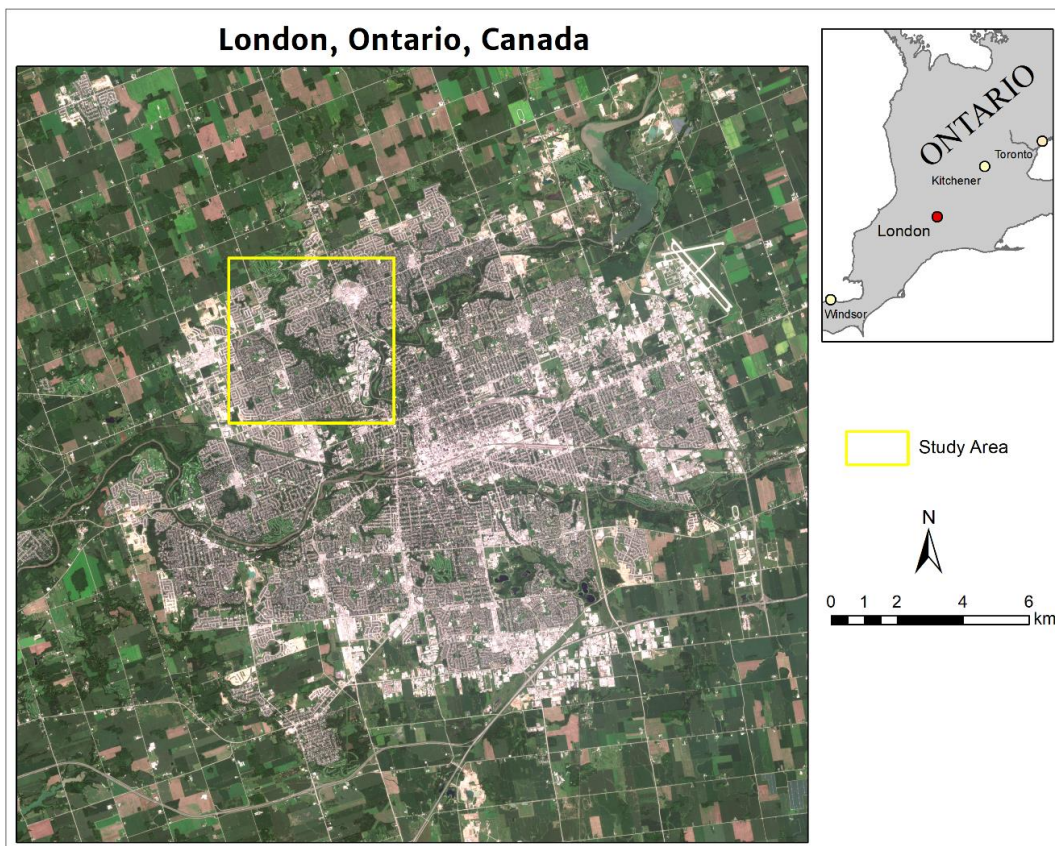
Figure 2.1: Study area within London, Ontario

The study made use of a Geoeye-1 image captured on July 9, 2018. Geoeye-1 is a satellite mounted high-resolution multispectral sensor owned by the company DigitalGlobe. The satellite is in sun-synchronous orbit at 684 km and makes 12 to 13 orbits daily. It contains four bands corresponding to blue, green, red and near-infrared (NIR) wavelengths (Table 2.1). The multispectral bands have a spatial resolution of 1.6 m. Additionally, there is a panchromatic band with a spatial resolution of 0.4 m.

Table 2.1: Geoeye-1 imagery specifications

Band #	Wavelength (nm)	Colour	Spatial Resolution (m)
Band 1	450-510	Blue	1.6
Band 2	510-580	Green	1.6
Band 3	655-690	Red	1.6
Band 4	780-920	Near Infrared	1.6
Panchromatic	450-800	Greyscale (covers visible spectrum to beginning of NIR)	0.4

The study's lidar data was collected on May 15, 2017 using an aircraft mounted Leica ALS70-HP. This sensor is produced by Leica Geosystems. The study area data is part of a larger lidar dataset of Southwestern Ontario around Lake Erie and is collected and provided by the Ministry of Agriculture, Food and Rural Affairs (OMAFRA). The average lidar point density is 8 points/m^2 and the wavelength of the laser is 1064 nm. Each lidar pulse may have up to five returns.

2.2.2   Class Selection

There are numerous tree species in the study area, both native and introduced. The city's tree inventory accounts for many city-maintained trees, including most street trees and some park trees. Within the study area, this includes over 160 species. Classification was performed to differentiate between five tree types. Four species were selected: *Acer platanoides* (Norway maple), *Tilia cordata* (littleleaf linden), *Picea pungens* (Colorado blue spruce) and *Gleditsia triacanthos* (honey locust). In addition, the Norway maple cultivar "Schwedleri" was also selected. These species are among the ten most common in the study area, according to the city tree inventory. However, they are also all introduced species which do not grow natively in the London area. In addition, they have

marked physical differences. Colorado blue spruce is the only conifer of the five and has blue-green coloured needles. The leaf and crown shapes of Norway maple, littleleaf linden and honey locust are all distinct. Norway maple and Schwedleri Norway maple have the same crown and leaf shape, but "Schwedleri" is distinguished by red coloured foliage (Figure 2.2).

Figure 2.2: Trees classified in study. Clockwise from top left: Norway maple, Schwedleri Norway maple, Colorado blue spruce, littleleaf linden, honey locust.

2.2.3 Workflow

The general stages of processing are shown in the flowchart below (Figure 2.3). Classification began with preprocessing Geoeye imagery through atmospheric correction and orthorectification. The lidar point cloud was also processed to generate elevation

products including a normalized digital surface model (nDSM). The nDSM was the basis of watershed delineation, which created the tree crown objects used in the study. Shaded relief elevation images were also created from the nDSM. The Geoeye image was further processed by pansharpening (increasing resolution to panchromatic band pixel size of 0.4 m). The pansharpened bands were used to generate GLCM texture measures. Additionally, GLCM textures were generated from the nDSM and four shaded relief images. The original 1.6 m Geoeye bands were masked based on NDVI and bright pixels (sunlit) to ensure only tree vegetation reflectance was measured. From these new images (masked Geoeye images, GLCM texture for pansharpened Geoeye bands, shaded relief and nDSM) zonal statistics in ArcGIS was run to calculate features from the pixels in the tree crown object. Additionally, LAS Canopy was used to calculate metrics from the lidar points within the tree crown object boundaries. This provided all the features used for classification in this study. More detailed explanations for each stage are provided in the following subsections.
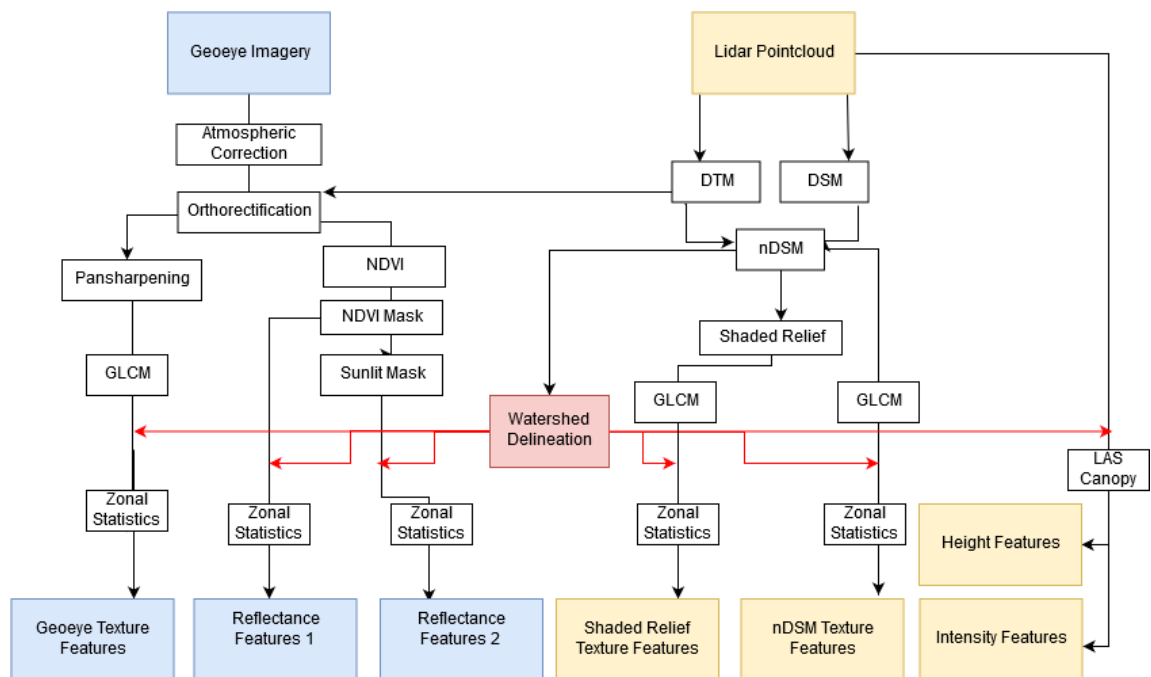
Figure 2.3: General workflow for creation of classification features. Features derived from imagery are in blue, from lidar in yellow.

2.2.4 Object Creation

This study used object-based classification, where pixels representing the same feature are grouped together as an object and assigned the same class. Here, the objects represent individual tree crowns. Segmentation of tree crown objects was performed using marker-controlled watershed segmentation from the R Forest Tools package (Plowright 2018).

The algorithm delineates tree crowns from an nDSM, which represents the height of objects as if they were on a level plane, without the influence of terrain elevation. The nDSM was generated from lidar. A digital surface model (DSM) was generated based on the highest elevation lidar point for each cell, while a digital terrain model (DTM) was generated based on the average elevation of ground lidar points in each cell. The DTM was then subtracted from the DSM to obtain the nDSM.

Marker controlled watershed segmentation uses a search window to find local maxima and delineates the "watershed" around them. Here, the local maxima represent the tops of trees. Tree crowns tend to increase in size alongside tree height. A more accurate segmentation can be achieved by changing the size of the search window in relation to the elevation value of the pixel (Chen et al. 2006). To establish how crown size varies with height, 105 trees of several common species were manually delineated. Their maximum height and crown width were recorded and a curve was plotted through these points to establish a function between tree height and crown size (Chen et al. 2006). This resulted in under-segmentation, with several smaller crowns being merged together. To avoid this problem, a new function was generated using only the smallest crown for each 1 m height interval.

Segmentation was performed using three nDSMs of various pixel sizes (1 m, 1 m with low-pass filter, 0.5 m, 0.5 m with low-pass filter). The low-pass filter was used to fill gaps and irregularities in crowns, which were particularly noticeable in the 0.5 m image (Barnes et al. 2017). The unfiltered 0.5 raster produced poor results and was not further analyzed. From visual examination, height differences between crowns were

noticeable at both resolutions, but differences within crowns were emphasized more strongly with 0.5 m pixel size.

The generated crowns were compared to manually delineated crowns to determine segmentation quality (Figure 2.4). The sections of generated crowns that intersected manual crowns were extracted, with each containing three measurements of area: the area of the manual crown, the area of the original generated crown, and the area of the section of the generated crown that intersects the manual crown.
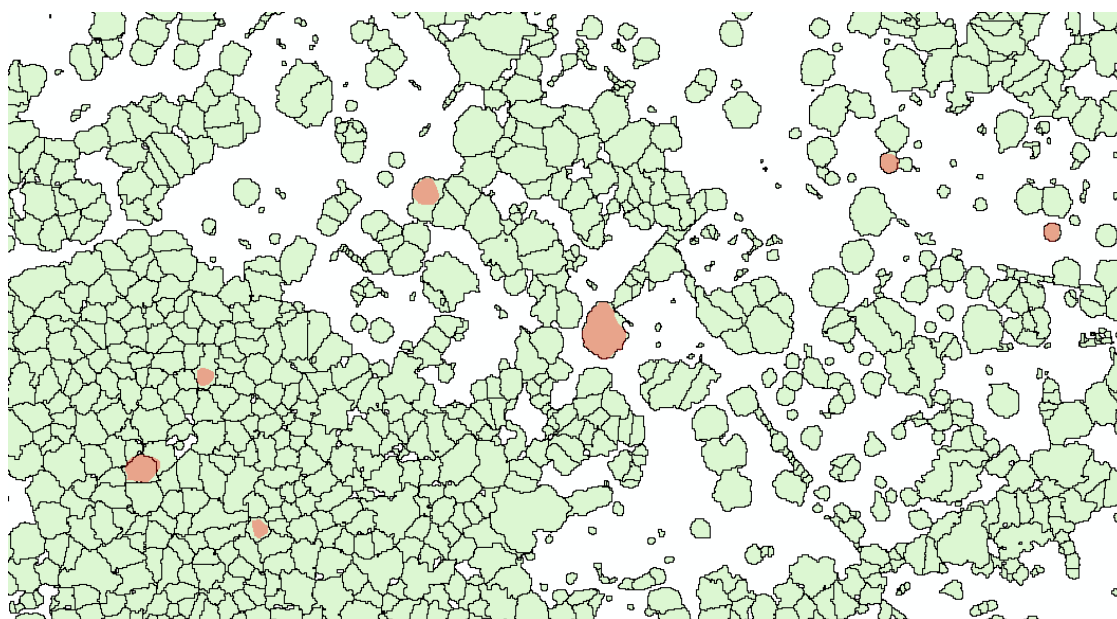
Figure 2.4: Manual crowns (red) and generated crowns (green)

Three metrics for segmentation quality were then created:

1) The total number of generated crowns that intersect a manual crown. The number of intersecting generated crowns should be lower, as that indicates a single manual crown is not split between multiple generated crowns.

2) For each manual crown, the largest intersecting generated crown area divided by the total area of intersecting generated crowns. If there are multiple intersecting crowns, it is preferable that a single one cover most of the manual crown.

3) The area of the section of a generated crown that intersects a manual crown, divided by the total area of that generated crown. Ideally, the portion of the

generated crown intersecting the manual crown will be a similar size to the entire generated crown. If not, it indicates that multiple tree crowns are contained in the generated crown.

The metrics indicated that the low-pass filtered 0.5 m nDSM produced the best segmentation (Table 2.2). The 1 m low-pass filtered nDSM had fewer total intersecting generated crowns, indicating that single manual crowns were not split between multiple generated objects. However, the size of the part of the generated object that intersects with the manual crown was much smaller than the total size of that object, suggesting that the generated object represents multiple tree crowns. In contrast, the 0.5 m low-pass filtered nDSM, generated objects more often contained only a single tree crown. On average, the intersecting area of the generated object containing the manual crown made up 73.76% of the total area of the same generated object. Because of the higher quality of crowns based on the measurements, further processing made use of the objects generated by the 0.5 m low-pass filtered nDSM.

Table 2.2: Accuracy measures for tree crown objects. Best value in green. LP = low-pass filter. Metric 1 is the exact value, metric 2 is mean of values for all generated crowns that intersect a watershed object, metric 3 is mean of values for largest intersecting generated crown for each manual crown.

nDSM	Total # intersecting generated objects	Largest generated object as percent of all intersecting objects	Area of generated object intersecting with manual crown / Area of entire generated object
1m	130	88.89%	71.61%
1m LP	102	96.45%	59.93%
0.5m LP	112	94.27%	73.76%

2.2.5 Selection of Crowns for Classification

From the objects generated from watershed segmentation, 448 objects representing individual tree crowns were selected for classification (Table 2.3). The crowns represent trees of different ages and sizes throughout the study area. Because tree age can affect lidar intensity, an attempt was made to use trees of different ages for classification

(Korpela et al. 2010). The study area was divided into nine sections, based on the typical size of trees. Within each section, 55 points (11 points per tree type) were placed randomly. The nearest object of that point's target tree species was selected to be used in classification. The species was verified using Google Streetview images. Selection was limited to city-maintained trees identified by the city inventory, and only objects containing a single tree crown were used. This was to avoid confusion caused by a single object containing multiple trees of different species. However, it does mean that classification accuracy is likely higher than if all tree crowns in the study area were classified. In some cases, there was no tree near the random point, so the exact number of sample crowns differs between species. Selected crowns were distributed throughout the study area, but limited to mostly to residential areas (Figure 2.5)

Table 2.3: Number of crowns selected for classification per tree type.

Tree Type	Number of Crowns
Norway maple	92
Schwedleri Norway maple	82
Honey locust	92
Littleleaf linden	96
Colorado blue spruce	86
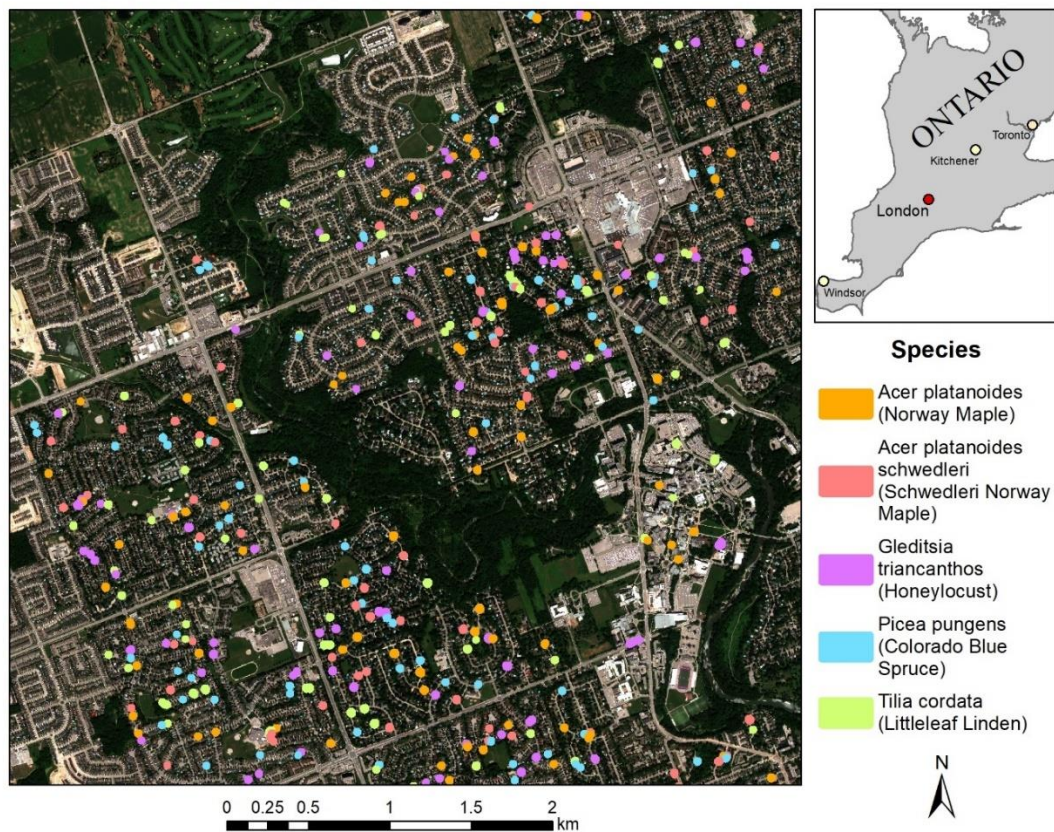
Figure 2.5: Selected tree crowns within the study area.

2.2.6 Image Processing

Further processing was required to generate the features used for classification from the imagery and lidar data. The Geoeye-1 image was provided without atmospheric correction or orthorectification. ATCOR atmospheric correction was performed in PCI Geomatica to remove atmospheric distortion in the image and transform pixel values into surface reflectance (ATCOR Ground Reflectance Tutorial). Additionally, orthorectification was performed using ENVI to adjust for distortion caused by elevation changes in the image, and to align properly with the tree crown objects and the nDSM from which they were delineated (Harris Geospatial. RPC Orthorectification Tutorial). Pansharpening was also performed, to enhance the resolution of multispectral Geoeye bands to that of the panchromatic resolution (0.4 m). This was done using the SPEAR pansharpening method in ENVI (Harris Geospatial. SPEAR Pansharpening).

From the Geoeye image, the mean and standard deviation (SD) for each of the four bands were found for each crown. Mean and SD were also calculated based on the normalized difference vegetation index (NDVI). NDVI is based on the difference between red and NIR band values and indicates healthy vegetation. The calculation was based on pixels that fall within the crown object. However, differing pixel sizes between the nDSM and the Geoeye image, as well as imperfect registration, meant that tree crown objects did not perfectly align with trees in the Geoeye image. Pixels representing other features would be included in metrics based on imagery. To avoid this problem, two masks were used. First, an NDVI mask was used to eliminate non-vegetation pixels. Pixels with a value below 0.5 were changed to no data, in order to avoid their inclusion when calculating metrics. Due to the high image resolution, there were large differences in pixel values within tree crowns caused by shadows. Past studies have indicated that selecting only sunlit pixels improves tree species classification (Immitzer, Atzberger, and Koukal 2012, Shen and Cao 2017). Once non-vegetation pixels were removed, a further mask was created by finding the mean NIR reflectance value of each crown, then changing all pixels falling below that value to no data (Figure 2.6). The remaining pixels were considered sunlit. (Shen and Cao 2017). The mean and SD were calculated twice, once with only the NDVI mask applied, and a second time with the sunlight mask applied as well. This was performed using the zonal statistics tool in ArcGIS, which finds a mean value based on pixels within a polygon (ESRI).
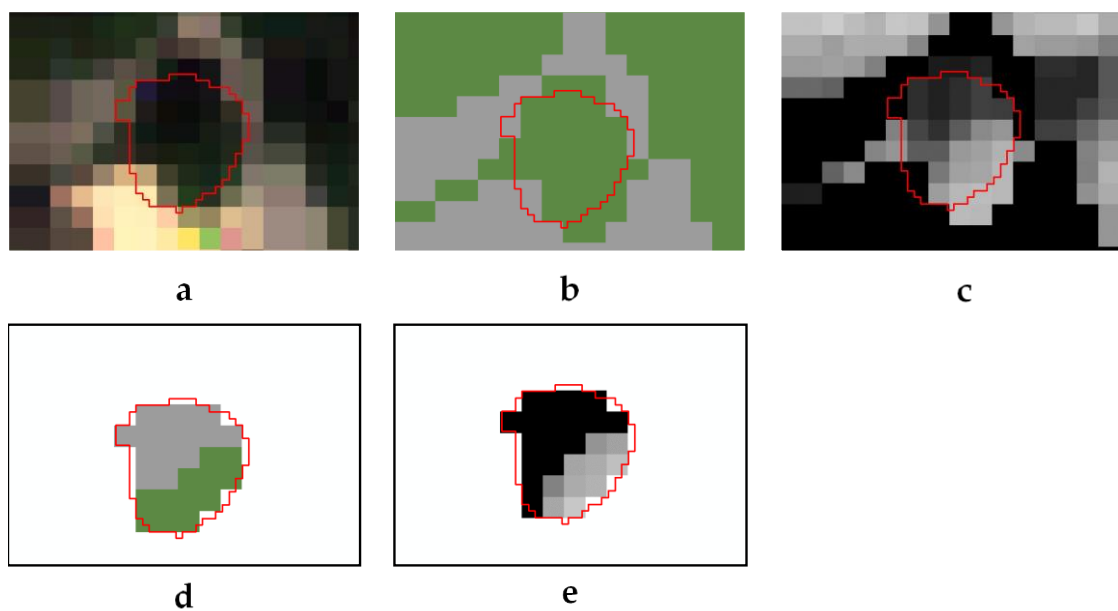
Figure 2.6: Process for extracting reflectance features: a) Geoeye-1 imagery with crown object overlying pixels. b) NDVI threshold, pixels over 0.5 NDVI in green, grey masked. c) NIR band, used for sunlit mask. d) Sunlit mask, pixels below mean NIR reflectance in crown masked out (grey). e) Remaining pixels after application of both masks.

2.2.7 Lidar Processing

Lidar features were created in LASTools software, with the use of LASCanopy (Rapidlasso). For each crown, the metrics were calculated based on lidar points within the bounds of the polygon (Figure 2.7). Points classified as ground or high/low noise were excluded, as were points which fell below a certain height (here left as the default value of 1.37 m). For both height and intensity, the same features were generated. These included exact values (minimum and maximum value of lidar points), statistics (mean, average square value, kurtosis, skewness, standard deviation) and percentiles. Height percentiles indicate that a certain percentage of lidar points fall below a certain height. Height percentiles were normalized to allow trees of different heights to be more directly comparable (e.g. 75% of points fall below 86% of the tree's maximum height, rather than 7.8 m) (Ørka, Næsset, and Bollandsås 2009). Intensity percentiles indicate that a certain

percentage of points have an intensity value lower than a certain value (e.g. 75% of points have an intensity value of less than 25000).

<p style="text-align:center">a   b</p>
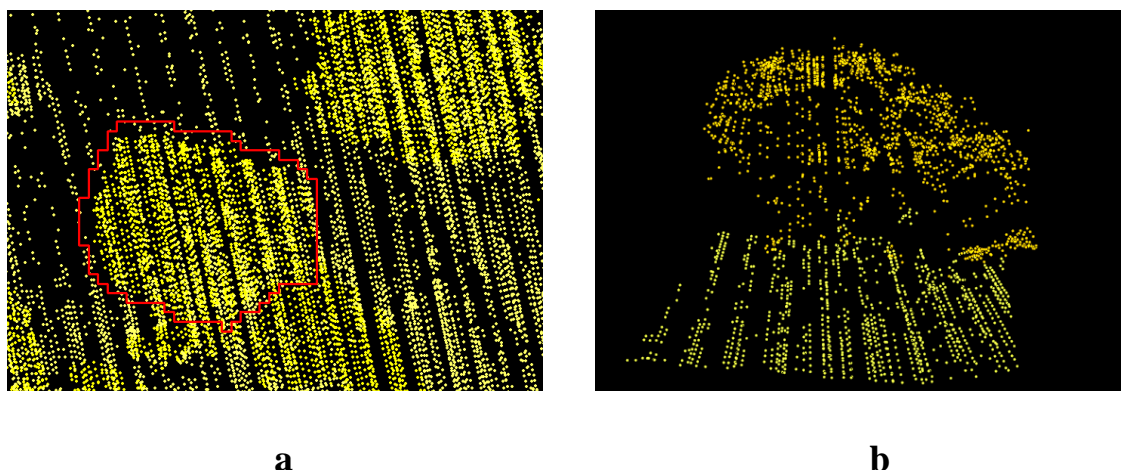
Figure 2.7: a) Lidar points viewed from above, with outline of crown shown. Lidar features calculated only for points within crown object. b) Lidar point cloud viewed from side, showing varying elevations of points. Points below 1.37 m excluded from calculations.

2.2.8   Texture Processing

Texture measures were generated using the TEX algorithm in PCI Geomatica (PCI Geomatics. TEX Texture Analysis). The window for texture calculation was set as 3x3 due to the presence of small trees with relatively few pixels comprising the crown. Eight GLCM measures, and four GLDV measures were calculated. The grey level co-occurrence matrix is created from pairs of pixel values between neighbouring pixels, while GLDV is based on the diagonal of the matrix (Hall-Beyer 2018). Textures were calculated based on the nDSM and all four Geoeye pansharpened bands.

Texture measures were also generated based on shaded relief images. Shaded relief is a visualization method that simulates the shadowing effect caused by differences in elevation and is typically used to represent surface roughness of terrain. In this study, the shadowing effect was instead used to exaggerate differences in pixel values of the nDSM for tree crowns. Shaded relief images for the four cardinal directions were

generated in ArcGIS using the nDSM, with sun azimuth at 0, 90, 180 and 270 degrees, and sun elevation at 45 degrees (Figure 2.8) Zonal statistics in ArcGIS was once again used to get a mean value for each texture measure. However, edges of trees had values that were influenced by the pixels surrounding the tree crown, rather than within crown pixel value differences. To exclude these, the tree crown polygons were decreased in size by 0.5 m on all sides (the size of one nDSM pixel).
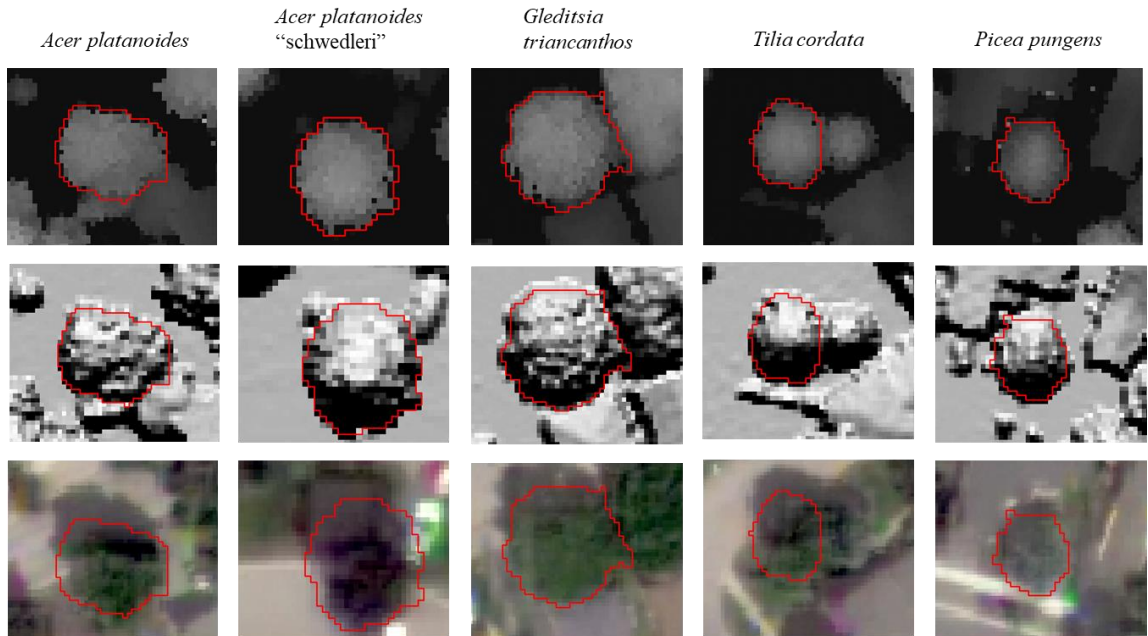
Figure 2.8: Data used to generate texture features, with example for each tree type. From top to bottom: nDSM, shaded relief, pansharpened Geoeye-1 imagery. Note that the tree crown object goes along edges of trees. For this reason, reduced sized objects were used for the calculation of texture features.

In total, 160 classification features for each tree crown were generated (Figure 2.9 and Figure 2.10). For full descriptions of these features, see Appendix A.
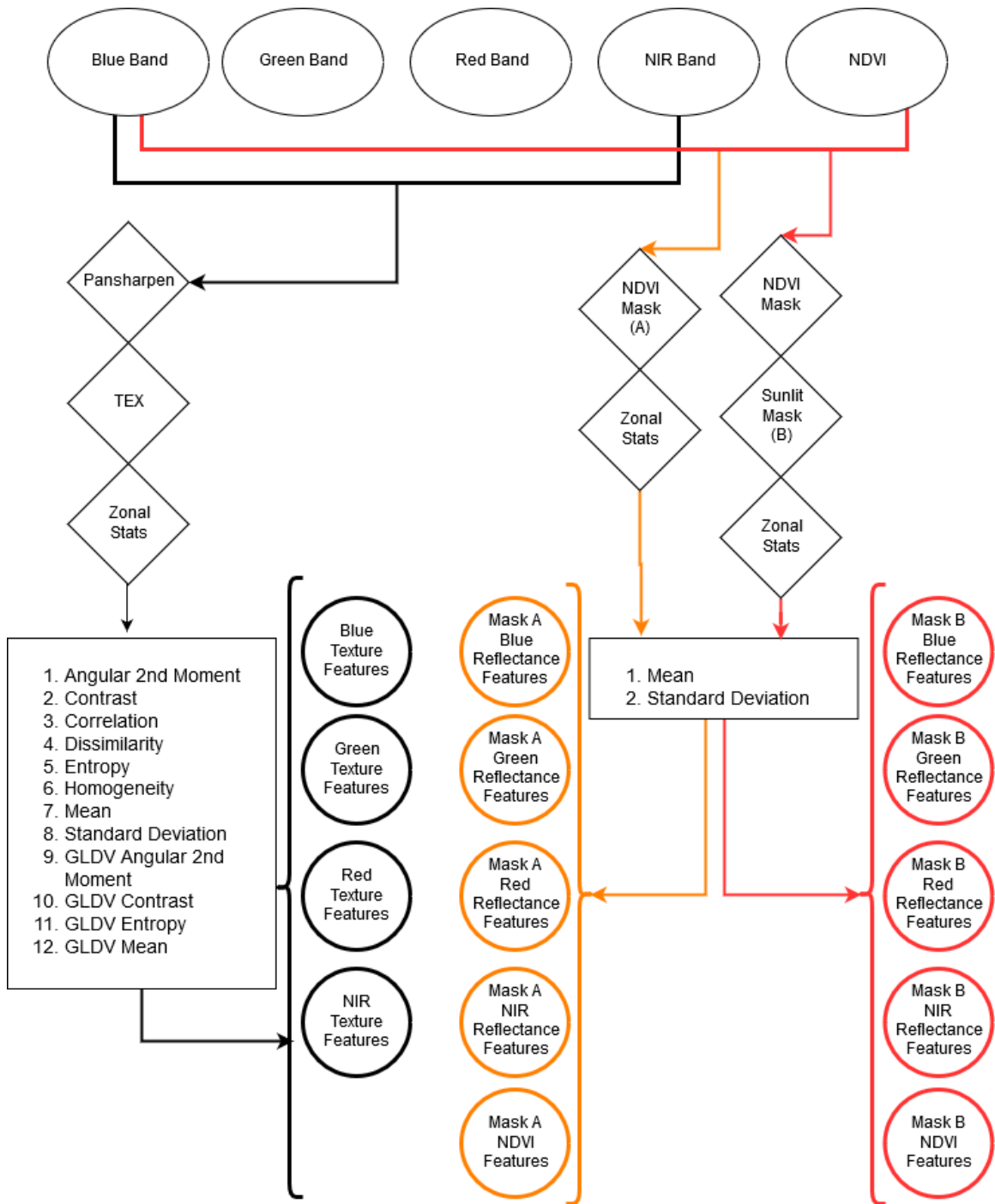
Figure 2.9: Features derived from Geoeye-1 imagery. Black: Texture features. Orange: Reflectance features (NDVI mask). Red: Reflectance features (Sunlit mask).
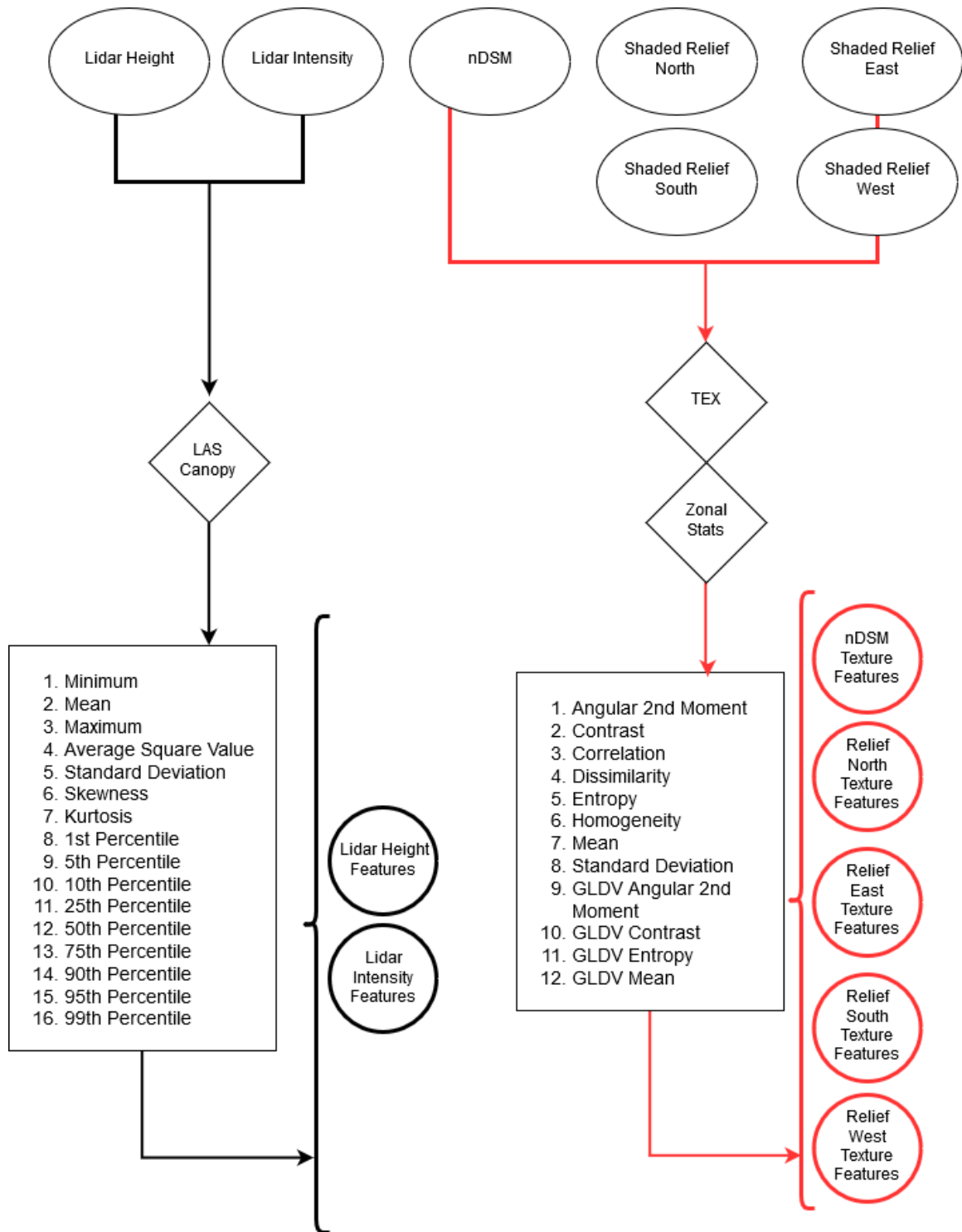
Figure 2.10: Features derived from lidar data. Black: Lidar height and intensity features from point cloud. Red: Texture features from lidar derived nDSM and shaded relief.

2.2.9   Support Vector Machine Classification

Classification was performed using support vector machine (SVM) which is a machine learning classifier. SVM finds the best fitting hyperplane to separate two classes. Typically, a linear separation is not possible, so the data is transformed to a higher dimension where a separation can be made. This requires the use of a kernel, such as the radial basis function which is used in this study. Additionally, SVM is a binary classifier for separating two classes, so various methods have been developed to allow multiclass classification (Pu 2017). This study used the SVM implementation in the R package "e1071", which uses the one-against-one technique (Meyer 2019). For each feature to be classified this method tries all possible binary combinations of classes and assigns the feature to the class which it is most often placed in (Gidudu, Hulley, and Marwala 2007).

SVM has several benefits for classification. In this study 160 features were tested, with up to 88 being used at a time, while only 448 tree crowns were available as training and testing data. With SVM, classification accuracy is not negatively affected by high dimensionality (Pu 2017). Additionally, it can perform well with a relatively small amount of training data (Fassnacht et al. 2016). The use of random forest classification was also considered, but ultimately SVM was chosen as it performed better in several tree classification studies (Immitzer, Atzberger, and Koukal 2012, Dalponte, Bruzzone, and Gianelle 2012, Adelabu et al. 2013, Shang and Chisholm 2014).

Once classification was performed, the results were compared to the true classes of the testing data. From the comparison of predicted and actual classes, a confusion matrix was generated (Table 2.4). Each column of the matrix shows what the training data was classified as. The mean of each column is the producer's accuracy of the class, indicating how many testing samples were classified correctly for a particular class. The rows show to which class members of a predicted class truly belong. The mean of each row is the user's accuracy. The sum of the diagonals divided by the total number of samples gives the overall accuracy, representing the percent of testing samples classified correctly (Lillesand, Kiefer, and Chipman 2008).

Table 2.4: Example confusion matrix. Classes A through E. Columns indicate the reference classes, while rows indicate the predicted classes. Column total is producer's accuracy for that class, row is user's accuracy. Overall accuracy in red is the sum of the diagonals divided by the total number of samples

	A	B	C	D	E	Total	UA
A	71	19	2	2	2	96	0.739583
B	13	56	2	0	5	76	0.736842
C	4	3	86	0	5	98	0.877551
D	1	0	0	84	0	85	0.988235
E	3	4	2	0	84	93	0.903226
Total	92	82	92	86	96	448	
PA	0.771739	0.682927	0.934783	0.976744	0.875		0.850446

In order to have better confidence in the results, five-fold cross validation was used. This method involves splitting the data into five groups, with the classes distributed evenly between the groups. Classification is run five times, using four groups as training data and one group as testing data. Each of the five groups is used once as testing data. The final overall accuracy (OA) is the mean of the overall accuracy from the five iterations (Rodríguez, Pérez, and Lozano 2010).

Initially, classification was performed with single features. This was to determine which were most useful for classification and guide the selection features to group together later on. Each of the 160 features were used as the sole classification feature, and the resulting overall accuracy was recorded. Next, groups of related features were tested. The different combinations of features were based on the data source, the type of feature, and the results of single feature classification (e.g. removing low performing features). Following this, the best results of group classification were combined. In total, 75 different combinations of features were tested. The main groups of features are as follows:

1) Imagery pixel values

2) Imagery texture measures

3) nDSM texture measures

4) shaded relief texture measures

5) lidar height features

6) lidar intensity features.

2.3 Results

2.3.1 Single Feature Results

Intensity features performed far better than features from any other group (Table 2.5). The top seven most accurate single feature classification results came from intensity metrics. The 75th percentile of intensity had the highest classification accuracy at 63.42%, which outperforms entire groups of features (i.e. Geoeye reflectance, height features, nDSM texture). Other intensity features with high accuracy included statistical metrics (mean, skew and standard deviation) as well as middle range percentiles (25th – 90th). Percentiles at the upper and lower ends were less useful, as was the minimum intensity value. The maximum and 99th percentile of intensity were almost always the same value, and of no use for distinguishing species.

Table 2.5: Classification overall accuracy using single lidar intensity feature.

Intensity Feature	OA		Intensity Feature	OA
75th Percentile	63.42%		10th Percentile	42.20%
50th Percentile	62.09%		95th Percentile	39.08%
Mean	55.38%		5th Percentile	39.07%
Skewness	52.48%		Kurtosis	36.38%
90th Percentile	49.10%		Minimum	33.03%
25th Percentile	48.73%		Average Square	25.24%
Standard Deviation	44.43%		99th Percentile	21.89%
1st Percentile	42.41%		Maximum	21.43%

Among height features, middle range height percentiles (50th and 75th) classified trees most accurately, which is similar to results found in Liu et al. 2017 (Table 2.6). Percentiles at extremes (1st, 99th) were less accurate. The skew and kurtosis of height had higher accuracy than other statistics. The minimum height outperformed the maximum height, which was not useful as each species was represented by trees of different ages (and therefore heights).

Table 2.6: Classification accuracy using single lidar height feature.

Feature	OA		Feature	OA
50th Percentile	41.32%		1st Percentile	29.94%
75th Percentile	40.44%		Kurtosis	29.27%
25th Percentile	35.93%		Minimum	28.33%
10th Percentile	34.16%		99th Percentile	28.15%
5th Percentile	32.58%		Standard Deviation	25.22%
Skewness	32.58%		Maximum	21.39%
90th Percentile	30.58%		Mean	21.18%
95th Percentile	30.38%		Average Square	19.40%

For Geoeye, mean NIR band reflectance was the most useful feature with 42.17% overall accuracy (Table 2.7). Next followed mean green band reflectance, mean NDVI, and the standard deviation of NIR. Red and blue band mean reflectance were lower, as were most standard deviation measurements. Vegetation reflectance is somewhat higher in green wavelengths than in blue or red, and near-infrared reflectance is much higher. The higher classification accuracy of these bands is similar to Immitzer et al. 2012 and Li et al. 2015, which both found green and NIR in Worldview-2 to be useful but differs as Immitzer also found the blue band to be important.

Table 2.7: Classification accuracy using single Geoeye-1 reflectance feature.

Sunlit Mask Feature	OA		NDVI Mask Feature	OA
NIR Mean	42.17%		NIR Mean	39.72%
Green Mean	31.94%		NIR SD	31.05%
NDVI Mean	31.49%		NDVI Mean	30.16%
NIR SD	26.83%		Green Mean	27.92%
Red Mean	25.23%		Red Mean	25.28%
Blue Mean	24.80%		NDVI SD	25.22%
Red SD	22.09%		Blue Mean	23.49%
NDVI SD	21.87%		Red SD	22.13%
Green SD	21.41%		Green SD	19.18%
Blue SD	20.52%		Blue SD	18.09%

The results from texture measures were fairly similar for all shaded relief directions as well as the nDSM (Table 2.8 and Table 2.9). Texture measures which had high accuracy across all shaded relief directions and the nDSM included standard

deviation, dissimilarity and GLDV mean. GLCM mean and correlation were not useful. Dissimilarity and variance both relate to "the dispersion of value around the mean" (Hall-Beyer 2018). Both textures emphasize edges, where pixel values change rapidly (Hall-Beyer 2017). This suggests that crown height changes help differentiate species. These changes occur within a 3x3 pixel (1.5 m x 1.5 m) window, representing changes over fairly large sections of the tree crown. GLDV mean is equivalent to dissimilarity, so its comparable accuracy is expected (PCI Geomatics. TEX Texture Analysis). The low performing GLCM mean and correlation both are interior measures, for areas of similar pixel values (Hall-Beyer 2017). The lack of homogenous areas in the tree crowns of all species may explain their low classification accuracy.

Table 2.8: Classification accuracy using single shaded relief texture feature.

North Relief Feature	OA		East Relief Feature	OA
Standard Deviation	36.63%		Standard Deviation	42.01%
Dissimilarity	36.42%		Contrast	39.51%
GLDV Mean	36.42%		GLDV Contrast	39.51%
Contrast	35.99%		Dissimilarity	38.64%
GLDV Contrast	35.99%		GLDV Mean	38.64%
Angular 2nd Moment	35.74%		GLDV Entropy	37.29%
GLDV Ang. 2nd Moment	35.51%		Homogeneity	36.16%
Homogeneity	35.49%		Entropy	35.73%
Entropy	35.49%		GLDV Ang. 2nd Moment	35.06%
GLDV Entropy	35.25%		Angular 2nd Moment	34.15%
GLCM Mean	29.88%		Correlation	28.58%
Correlation	20.77%		GLCM Mean	28.41%
South Relief Feature			West Relief Feature	
Standard Deviation	40.58%		Dissimilarity	42.44%
GLDV Entropy	40.43%		GLDV Mean	42.44%
Dissimilarity	39.48%		Homogeneity	39.69%
GLDV Mean	39.48%		GLDV Entropy	39.04%
GLDV Ang. 2nd Moment	39.30%		GLDV Angular 2nd Moment	39.04%
Contrast	39.25%		Standard Deviation	38.88%
GLDV Contrast	39.25%		Contrast	38.43%
Angular 2nd Moment	38.65%		GLDV Contrast	38.43%
Entropy	38.44%		Angular 2nd Moment	37.73%
Homogeneity	37.54%		Entropy	37.71%
GLCM Mean	37.03%		GLCM Mean	31.00%
Correlation	26.13%		Correlation	21.88%

Table 2.9 Classification accuracy using single nDSM texture feature.

nDSM Feature	OA
Standard Deviation	40.58%
Dissimilarity	40.13%
GLDV Mean	40.13%
GLDV Entropy	39.47%
GLDV Ang. 2nd Moment	38.35%
Homogeneity	37.04%
Entropy	35.24%
Contrast	35.22%
GLDV Contrast	35.22%
Angular 2nd Moment	33.90%
Correlation	30.37%
GLCM Mean	19.86%

The results of classification with textures created from Geoeye image bands differed from shaded relief and nDSM texture results (Table 2.10). GLCM mean, which was of little use with nDSM and shaded relief-based texture had the highest classification accuracy for all four bands. The GLCM mean is the mean of pixel value combinations in the GLCM matrix (Hall-Beyer 2018). Mean is high in cases where there are few edges with large pixel value differences (Hall-Beyer 2017). Angular second movement and correlation were the least accurate for visible spectrum bands. However, correlation produced a relatively high accuracy with NIR. High correlation indicates that there is a predictable relationship between neighbouring pixels (Hall-Beyer 2018).

Table 2.10: Classification accuracy using single Geoeye-1 texture feature.

Blue Texture	OA		Green Texture	OA
GLCM Mean	35.94%		GLCM Mean	38.86%
Contrast	35.48%		Homogeneity	36.61%
GLDV Contrast	35.48%		Dissimilarity	35.25%
Standard Deviation	34.39%		GLDV Mean	35.25%
Dissimilarity	33.49%		GLDV Ang. 2nd Moment	34.84%
GLDV Mean	33.49%		GLDV Entropy	34.83%
GLDV Ang. 2nd Moment	30.16%		Standard Deviation	33.46%
GLDV Entropy	29.27%		Contrast	33.01%
Homogeneity	28.13%		GLDV Contrast	33.01%
Entropy	24.11%		Entropy	31.03%
Correlation	22.55%		Angular 2nd Moment	30.10%
Angular 2nd Moment	22.29%		Correlation	23.68%
Red Texture	OA		NIR Texture	OA
GLCM Mean	33.71%		GLCM Mean	44.24%
Contrast	32.35%		Correlation	33.69%
GLDV Contrast	32.35%		Contrast	32.15%
Dissimilarity	31.92%		GLDV Contrast	32.15%
GLDV Mean	31.92%		Dissimilarity	29.49%
Standard Deviation	29.90%		GLDV Mean	29.49%
GLDV Entropy	28.14%		Standard Deviation	28.12%
GLDV Ang. 2nd Moment	27.92%		Angular 2nd Moment	26.14%
Homogeneity	25.88%		Entropy	25.68%
Entropy	22.98%		Homogeneity	23.42%
Angular 2nd Moment	22.55%		GLDV Ang. 2nd Moment	23.22%
Correlation	22.11%		GLDV Entropy	22.77%

2.3.2 Feature Group Results

For Geoeye imagery features, the highest classification accuracy came from using the means of all bands after masking out darker pixels with the sunlit mask (OA 60.03%) (Table 2.11). Including NDVI resulted in a slightly lower accuracy (OA 59.14%), as did including band standard deviations (58.11%). In most combinations of features, the set using the sunlit mask outperformed the matching set using only the NDVI mask. Band

standard deviations performed poorly and did not improve results. Including the NIR band substantially improved accuracy compared to using only the visible spectrum bands.

Table 2.11: Classification accuracy using multiple Geoeye-1 reflectance features. RGB = features from red, blue and green bands. Mask indicates whether sunlit mask or NDVI mask used.

RGB Mean	NIR Mean	NDVI Mean	RGB SD	NIR SD	NDVI SD	Overall Accuracy	Mask
✓	✓					60.03%	Sun
✓	✓	✓				59.14%	Sun
✓	✓		✓	✓		58.11%	Sun
✓	✓	✓	✓	✓	✓	57.67%	Sun
✓	✓					57.40%	NDVI
✓	✓		✓	✓		57.17%	NDVI
✓	✓	✓	✓	✓	✓	56.95%	NDVI
✓	✓	✓				56.51%	NDVI
✓						45.38%	Sun
✓			✓			43.36%	Sun
✓						38.66%	NDVI
✓			✓			37.77%	NDVI
			✓	✓		28.83%	NDVI
			✓	✓		24.35%	Sun
			✓			21.87%	Sun
			✓			19.42%	NDVI

It was unclear whether using texture measures of shaded relief was preferable to using texture measures of the nDSM. Textures from single shaded relief directions had lower accuracy than from the original nDSM. Combining all shade direction textures had a somewhat higher accuracy (OA 59.6%) than nDSM textures (OA 56.13%). This was also true for four of the five iterations of classification (Table 2.12). However, when combined with other feature groups, nDSM textures somewhat outperformed shaded relief textures. Excluding low performing texture measures based on the results of single feature classification did not improve accuracy compared to using all texture measures.

Table 2.12: Overall accuracy for each cross-fold validation run for nDSM and shaded relief features. Higher result in green.

Fold	nDSM	Shaded Relief
1	56.70%	61.80%
2	57.61%	63.04%
3	55.68%	62.50%
4	58.43%	57.30%
5	52.22%	53.33%
Average	56.13%	59.60%

Texture derived from Geoeye imagery performed better than either nDSM or shaded relief texture (Table 2.13). Texture from the NIR band (OA 53.17%) and the green band (OA 50.89%) outperformed texture from the red (OA 41.72%) and blue (OA 41.08%) bands. Classification using only textures from NIR and green achieved a better result (OA 71.68%) than using textures from all four bands (OA 68.94%).

Table 2.13: Classification accuracy using texture measures from Geoeye-1.

Blue Texture	Green Texture	Red Texture	NIR Texture	Overall Accuracy
	✓		✓	71.68%
✓	✓	✓	✓	68.94%
			✓	53.17%
	✓			50.89%
		✓		41.72%
✓				41.08%

Lidar height features performed best when percentiles and statistics were used together (OA 48.4%) (Table 2.14). Including exact values resulted in a lower accuracy (OA 44.7%). The same was true when comparing intensity percentiles and statistics (OA 69.5%) to all intensity features (68.6%).

Table 2.14: Classification accuracy when using lidar height and intensity features.

Height Exact	Height Stats	Height Percentiles	Intensity Exact	Intensity Stats	Intensity Percentiles	Overall Accuracy
				✓	✓	69.51%
			✓		✓	69.47%
			✓	✓	✓	68.59%
					✓	67.21%
			✓	✓		64.56%
				✓		63.89%
			✓			59.62%
	✓	✓				48.46%
✓		✓				45.35%
✓	✓	✓				44.70%
		✓				44.66%
	✓					43.55%
✓						35.08%

The results showed that lidar alone is able to classify the five types of trees with moderate accuracy. Using different groups of features derived from lidar data improved classification accuracy. While intensity features had 69.5% overall accuracy, this increased to 73.03% when both intensity and height features were used, and further increased to 77.73% when texture from the nDSM was included. Classification accuracy is further improved by incorporating imagery features. Including Geoeye mean reflectance and GLCM textures further improved overall accuracy to 85.1%. When using features from Geoeye, the overall accuracy when using only texture measures (OA: 71.68%) was almost as high as when using mean reflectance alongside texture measures (71.85%).

The features used in the most accurate classification were as follows: Geoeye reflectance means for all bands (limited to sunlit pixels), lidar intensity and height percentiles and statistics (minimum and maximum excluded), nDSM derived texture measures and Geoeye texture measures from the green and near-infrared bands (Table 2.15).

Table 2.15: Classification accuracy when using combined groups of features.

Geoeye Reflectance	Geoeye Texture	nDSM Texture	Shaded Relief Texture	Lidar Height	Lidar Intensity	Overall Accuracy
✓	✓	✓		✓	✓	85.08%
	✓	✓		✓	✓	84.65%
✓	✓		✓	✓	✓	83.72%
	✓		✓	✓	✓	82.61%
	✓			✓	✓	81.74%
✓				✓	✓	78.39%
		✓		✓	✓	77.73%
			✓	✓	✓	76.80%
	✓	✓				73.68%
				✓	✓	73.03%
✓	✓					71.85%
	✓					71.68%
					✓	69.51%

2.3.3 Species

The producer's and user's accuracy of individual species varied between feature groups (Figure 2.11 and Figure 2.12). Additionally, confusion between classes also differed based on the features used for classification (see Appendix B). Geoeye features produced good results for Norway maple and Schwedleri Norway maple, poorer results for Colorado blue spruce and littleleaf linden and worst results for honey locust. When looking at individual band results, Schwedleri Norway maple was classified very poorly in all bands except for green, where classification was still fairly low. It was still misclassified as littleleaf linden and Norway maple despite the difference in colour. The benefits of multispectral imagery for distinguishing species is greatest when all four bands are used.

The accuracy of species when classified using nDSM textures were similar. Colorado blue spruce was classified best, which is unsurprising considering its distinctive canopy shape. More confusion occurred between different deciduous species. Schwedleri

Norway maple had the lowest PA, but surprisingly was confused more often with honey locust, which has a very different canopy shape and density, rather than with Norway maple which it differs from primarily in colour. Overall, confusion existed between all deciduous trees. It may be that the 0.5 m resolution of the nDSM is still not sufficient to resolve the differences in crown structure between deciduous species. Additionally, each pixel represents the highest lidar point within that area. The gaps in the canopy for species such as honey locust may not be represented well because of this. In contrast, the structure of Colorado blue spruce leads to a more distinct changes in canopy height.
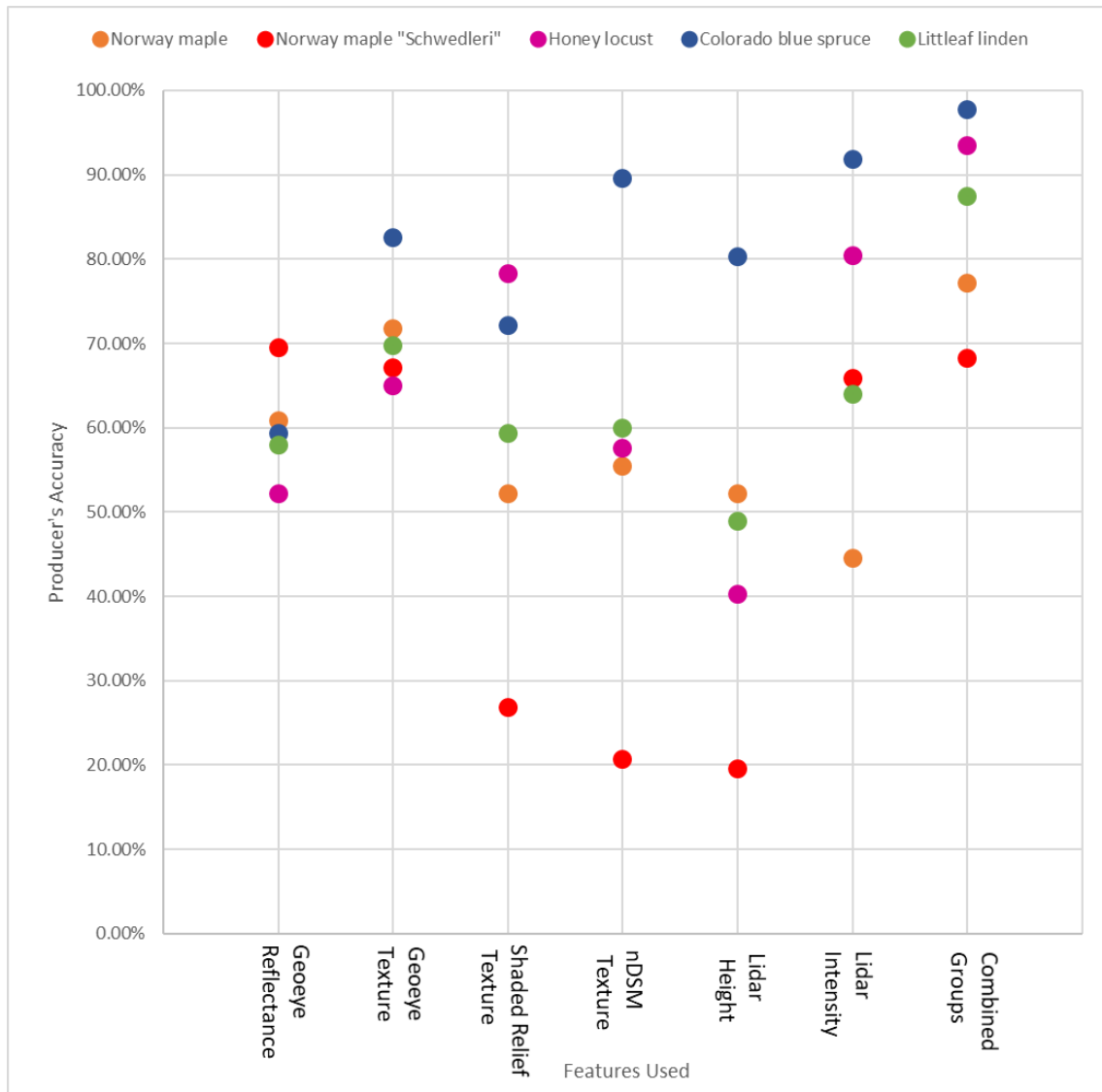
Figure 2.11: Producer's accuracy for all five tree types, when classified using different groups of features.
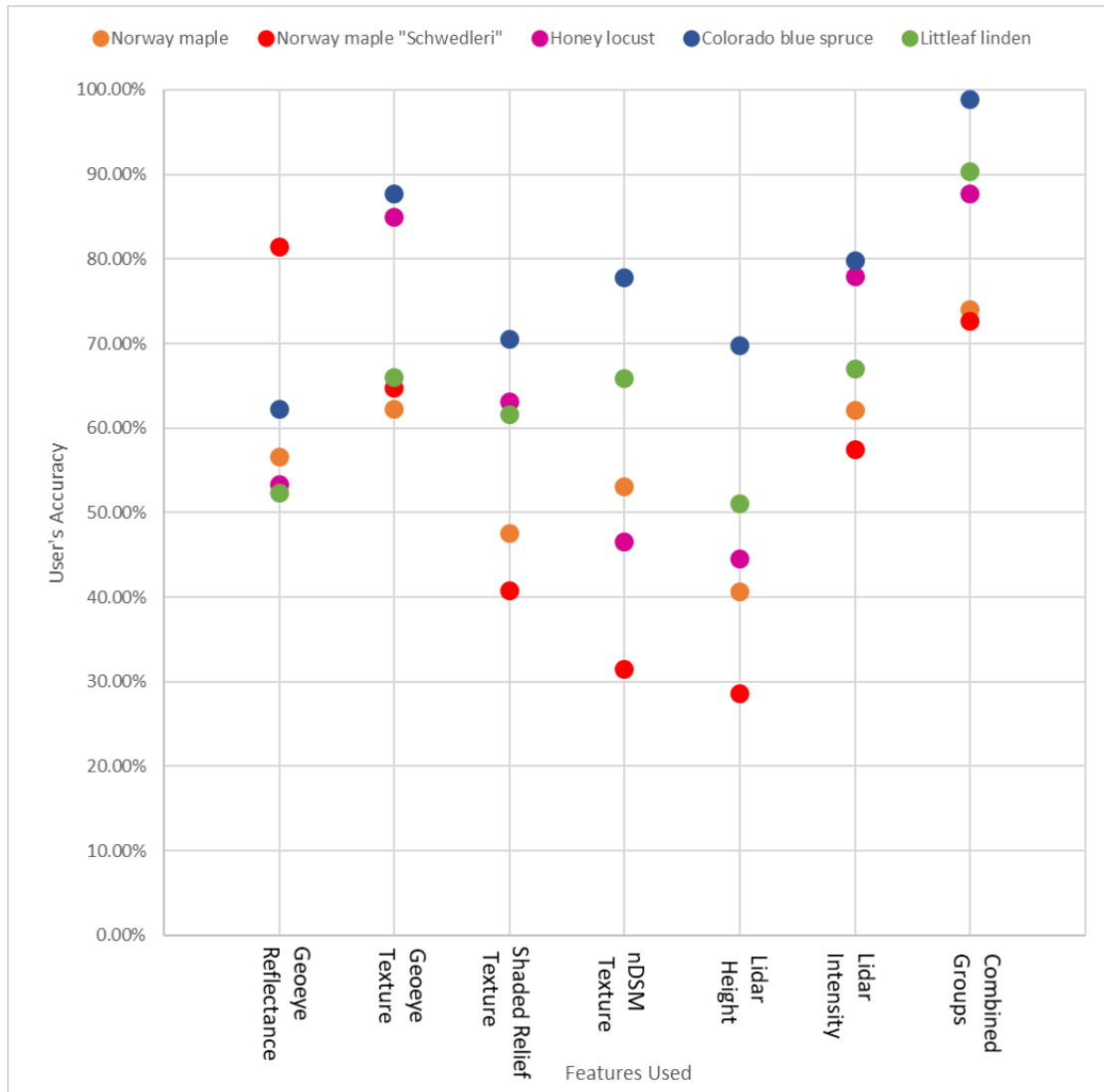
Figure 2.12: User's accuracy for all five tree types, when classified using different groups of features.

Texture measures of Geoeye green and NIR bands also classified Colorado blue spruce most accurately. The four deciduous tree types all had similar PA and were occasionally confused with each other. However, classification accuracy was fairly good for all species when using texture measures. Compared to texture from the nDSM, Geoeye texture was based off a higher resolution raster (0.4 m) and better represented shadowing than what was simulated by the coarser resolution shaded relief.

Using only metrics from lidar height classified Colorado blue spruce most accurately, while Schwedleri Norway maple had very low PA. The high accuracy of Colorado blue spruce is as expected due to its distinctive structure and foliage. However, Schwedleri Norway maple was confused fairly evenly with other species, not just Norway maple, which would have been expected considering their similar structure.

As before, lidar intensity metrics most accurately classified Colorado blue spruce. Honey locust was also highly accurately classified. When using intensity metrics, confusion most often occurred between the two types of Norway maple. This may be due to similar reflectance of the NIR laser used by lidar, or structural aspects, as both affect lidar intensity measurements.

The best classification result, combing features from lidar and imagery, had nearly perfect PA and UA for Colorado blue spruce, fully differentiating it from deciduous species. Honey locust was the next most accurately classified (PA 93.5%). Schwedleri Norway maple had the lowest PA but was still close to 70%.

User's accuracy did not differ greatly from producer's accuracy. In some cases, there were noticeable differences between the two types of accuracy, such as higher user's accuracy than producer's accuracy for honey locust when Geoeye texture was used for classification, and lower user's accuracy compared to producer's accuracy for blue spruce for nDSM texture, lidar height and lidar intensity. Despite these differences, there were no cases where user's accuracy was a particular cause of concern in the results.

2.4 Discussion

Texture measures derived from Geoeye imagery were extremely useful. Using textures from the green and NIR bands resulted in higher accuracy than using image reflectance. When combined together, there is only a marginal increase to the Geoeye texture accuracy (OA 71.7% for texture features alone, OA 71.8% with texture and reflectance features). This could be due to correlation between Geoeye mean reflectance and texture measures. The highest performing GLCM texture is the GLCM mean. The Pearson's R correlation with mean reflectance for the green band is 0.73, while for the NIR band it is

0.84. The strong correlation between these features may result in little additional information being contributed when Geoeye-1 reflectance is added to classification.

The four image bands of Geoeye are limited in how well they can differentiate species when using only mean reflectance. However, hyperspectral imagery is less accessible than multispectral imagery, being mostly limited to airborne sensors rather than satellites (Transon et al. 2018). Using GLCM texture measures appears to be a useful way to improve tree species classification when only multispectral images are available. Ke, Quackenbush, and Im 2010 found varying levels of contribution to classification from image mean reflectance and texture measures. In many cases, mean image reflectance outperformed texture measures. This differs from this study, where only NIR mean reflectance produced a higher accuracy than the higher performing texture measures when using single feature classification. For all other bands several texture measures resulted in higher accuracy than mean reflectance. Heinzel and Koch 2012 found classification based on texture to perform somewhat worse than image reflectance. The difference may be due to the lower number of texture features used in that study, as well as basing texture measures on transformed intensity rather than the original reflectance values from each band.

The results from using lidar features highlighted the importance of lidar intensity for tree classification. Intensity features resulted in higher classification accuracy than features based on lidar height. The intensity of returns is affected by the structure of the tree crown, as well as how both leaves and branches reflect incoming light (Holmgren, Persson, and Söderman 2008). In contrast, height is limited to structural features such as the density of leaves and branches, which affect the ability of laser pulses to penetrate the crown (Ørka, Næsset, and Bollandsås 2009). Despite the greatest benefits coming from intensity, all three types of features derived from lidar (intensity, height, nDSM texture) improved classification accuracy. This suggests that they all provide unique information for differentiating tree species. The results from using shaded relief were not noticeably better than simply using the nDSM. However, measurements based on the pattern or extent of shadowing on tree crowns may be beneficial and would be worth further examination.

Removing features that performed poorly based on single feature classification had little impact on classification accuracy. The best result excluded certain low performing metrics such as the maximum and minimum of height and intensity. When these features were included, overall accuracy was 84.82%, only slightly lower than the best result of 85.08%. Feature selection using an algorithm, rather than manually selecting features may have resulted in slightly higher accuracy (Fabian E. Fassnacht et al. 2014). Although reducing the number of features is not necessary for accuracy, it would be beneficial for processing time. In the present study, only 448 trees were classified, so the number of features had little impact on run times. However, tens of thousands of trees were delineated in total within the study area. Processing times would be much larger, making feature reduction beneficial for faster classification.

Although a good overall accuracy was achieved, this is only the accuracy of the 448 trees selected for classification, representing five tree types. Attempting to include more species, which would be necessary for a full classification of urban trees, would be more difficult and may be beyond the capabilities of the available datasets. Factoring the accuracy of tree crown delineation into classification accuracy would also be beneficial.

2.5 Conclusions

This research assessed the capability of Geoeye-1 high resolution multispectral imagery and 8 points/m lidar data to classify trees through SVM classification. Five types of trees, with 448 tree crowns total, were used for classification. Multiple combinations of classification features were tested, with the best result having an overall accuracy of 85.08%.

Classification performed using different groups of features showed that GLCM texture measures of pansharpened Geoeye green and NIR bands classify trees with moderate accuracy (OA: 71.68%). This was higher than using the mean reflectance of all four Geoeye bands (OA: 60%). This demonstrates how making use of texture measures can compensate for the low spectral resolution of Geoeye images.

Features measuring intensity were by far the best features derived from lidar (OA: 69.51%). However, the use of metrics based on the height of points in the lidar cloud, as well as texture measures of an nDSM generated from lidar further improved accuracy when combined with intensity features (OA: 77.73%). Making full use of all that lidar data can provide improves classification results.

Combing features derived from imagery and lidar further increased classification accuracy. The highest overall accuracy (85.08%) was achieved from combining mean reflectance from imagery, image texture measures, measures of lidar height and intensity, and nDSM texture measures. This was an increase of 7.78 percentage points above using lidar alone. These features from lidar data and high-resolution multispectral imagery should be considered in further attempts to classify tree species.

2.6   References

Adelabu, Samuel, Onisimo Mutanga, Elhadi Adam, and Moses Azong Cho. 2013. "Exploiting Machine Learning Algorithms for Tree Species Classification in a Semiarid Woodland Using RapidEye Image." Journal of Applied Remote Sensing 7 (1): 073480. doi:10.1117/1.JRS.7.073480.

Almas, Andrew D., and Tenley M. Conway. 2016. "The Role of Native Species in Urban Forest Planning and Practice: A Case Study of Carolinian Canada." Urban Forestry and Urban Greening 17. Elsevier GmbH.: 54–62. doi:10.1016/j.ufug.2016.01.015.

Alonzo, M, B Bookhagen, and D A Roberts. 2014. "Urban Tree Species Mapping Using Hyperspectral and Lidar Data Fusion." Remote Sensing of Environment 148: 70–83. doi:Doi 10.1016/J.Rse.2014.03.018.

Barnes, Chloe, Heiko Balzter, Kirsten Barrett, James Eddy, Sam Milner, and Juan C. Suárez. 2017. "Individual Tree Crown Delineation from Airborne Laser Scanning for Diseased Larch Forest Stands." Remote Sensing 9 (3): 1–20. doi:10.3390/rs9030231.

Chen, Qi, Dennis Baldocchi, Peng Gong, and Maggi Kelly. 2006. "Isolating Individual Trees in a Savanna Woodland Using Small Footprint Lidar Data." Photogrammetric Engineering & Remote Sensing 72 (8): 923–932. doi:10.14358/PERS.72.8.923.

Cho, Moses Azong, Renaud Mathieu, Gregory P. Asner, Laven Naidoo, Jan van Aardt, Abel Ramoelo, Pravesh Debba, et al. 2012. "Mapping Tree Species Composition in South African Savannas Using an Integrated Airborne Spectral and LiDAR System." Remote Sensing of Environment 125. Elsevier Inc.: 214–226. doi:10.1016/j.rse.2012.07.010.

Coburn, C. A., and A. C.B. Roberts. 2004. "A Multiscale Texture Analysis Procedure for Improved Forest Stand Classification." International Journal of Remote Sensing 25 (20): 4287–4308. doi:10.1080/0143116042000192367.

Dalponte, Michele, Lorenzo Bruzzone, and Damiano Gianelle. 2012. "Tree Species Classification in the Southern Alps Based on the Fusion of Very High Geometrical Resolution Multispectral/Hyperspectral Images and LiDAR Data." Remote Sensing of Environment 123. Elsevier Inc.: 258–270. doi:10.1016/j.rse.2012.03.013.

ESRI. 2019. Zonal Statistics as Table. http://desktop.arcgis.com/en/arcmap/10.6/tools/spatial-analyst-toolbox/zonal-statistics-as-table.htm

Fassnacht, Fabian E., Carsten Neumann, Michael Forster, Henning Buddenbaum, Aniruddha Ghosh, Anne Clasen, Pawan Kumar Joshi, and Barbara Koch. 2014. "Comparison of Feature Reduction Algorithms for Classifying Tree Species with Hyperspectral Data on Three Central European Test Sites." IEEE Journal of Selected Topics in Applied Earth Observations and Remote Sensing 7 (6): 2547–2561. doi:10.1109/JSTARS.2014.2329390.

Fassnacht, Fabian Ewald, Hooman Latifi, Krzysztof Stereńczak, Aneta Modzelewska, Michael Lefsky, Lars T. Waser, Christoph Straub, and Aniruddha Ghosh. 2016. "Review of Studies on Tree Species Classification from Remotely Sensed Data." Remote Sensing of Environment 186: 64–87. doi:10.1016/j.rse.2016.08.013.

Gidudu, Anthony, Gregg Hulley, and Tshilidzi Marwala. 2007. "Image Classification Using SVMs: One-against-One Vs One-against-All." The 28th Asian Conference on Remote Sensing, 801–806. http://arxiv.org/abs/0711.2914.

Goodenough, David G., Andrew Dyk, K. Olaf Niemann, Jay S. Pearlman, Hao Chen, Tian Han, Matthew Murdoch, and Chris West. 2003. "Processing Hyperion and ALI for Forest Classification." IEEE Transactions on Geoscience and Remote Sensing 41 (6 PART I): 1321–1331. doi:10.1109/TGRS.2003.813214.

Hall-Beyer, Mryka. 2017. "Practical Guidelines for Choosing GLCM Textures to Use in Landscape Classification Tasks over a Range of Moderate Spatial Scales." International Journal of Remote Sensing 38 (5). Taylor & Francis: 1312–1338. doi:10.1080/01431161.2016.1278314.

Hall-Beyer, Mryka. 2018. "GLCM Texture: A Tutorial,". https://prism.ucalgary.ca/handle/1880/51900

Harris Geospatial. 2019. RPC Othorectification Tutorial. https://www.harrisgeospatial.com/docs/RPCOrthoTutorial.html

Harris Geospatial 2019. SPEAR Pansharpening. https://www.harrisgeospatial.com/docs/SPEARPanSharpening.html

Heinzel, Johannes, and Barbara Koch. 2012. "Investigating Multiple Data Sources for Tree Species Classification in Temperate Forest and Use for Single Tree Delineation." International Journal of Applied Earth Observation and Geoinformation 18 (1). Elsevier B.V.: 101–110. doi:10.1016/j.jag.2012.01.025.

Holmgren, J., Å Persson, and U. Söderman. 2008. "Species Identification of Individual Trees by Combining High Resolution LiDAR Data with Multi-Spectral Images." International Journal of Remote Sensing 29 (5): 1537–1552. doi:10.1080/01431160701736471.

Immitzer, Markus, Clement Atzberger, and Tatjana Koukal. 2012. "Tree Species Classification with Random Forest Using Very High Spatial Resolution 8-Band WorldView-2 Satellite Data." Remote Sensing 4 (9): 2661–2693. doi:10.3390/rs4092661.

Ke, Yinghai, Lindi J. Quackenbush, and Jungho Im. 2010. "Synergistic Use of QuickBird Multispectral Imagery and LIDAR Data for Object-Based Forest Species Classification." Remote Sensing of Environment 114 (6). Elsevier Inc.: 1141–1154. doi:10.1016/j.rse.2010.01.002.

Konijnendijk, Cecil C. 2005. Urban Forests and Trees. Edited by Cecil Konijnendijk, Kjell Nilsson, Thomas Randrup, and Jasper Schipperijn. Urban Forests and Trees. Berlin, Heidelberg: Springer Berlin Heidelberg. doi:10.1007/3-540-27684-X.

Korpela, Ilkka, Hans Ole Ørka, Matti Maltamo, Timo Tokola, and Juha Hyyppä. 2010. "Tree Species Classification Using Airborne LiDAR - Effects of Stand and Tree Parameters, Downsizing of Training Set, Intensity Normalization, and Sensor Type." Silva Fennica 44 (2): 319–339. doi:10.14214/sf.156.

Li, Dan, Yinghai Ke, Huili Gong, and Xiaojuan Li. 2015. "Object-Based Urban Tree Species Classification Using Bi-Temporal Worldview-2 and Worldview-3 Images." Remote Sensing 7 (12): 16917–16937. doi:10.3390/rs71215861.

Lillesand, Thomas M., Ralph W. Kiefer, and Jonathan Chipman. 2008. Remote Sensing and Image Interpretation. 6th ed. John Wiley & Sons.

Liu, Luxia, Nicholas C. Coops, Neal W. Aven, and Yong Pang. 2017. "Mapping Urban Tree Species Using Integrated Airborne Hyperspectral and LiDAR Remote Sensing Data." Remote Sensing of Environment 200 (July). Elsevier: 170–182. doi:10.1016/j.rse.2017.08.010.

Ørka, Hans Ole, Erik Næsset, and Ole Martin Bollandsås. 2009. "Classifying Species of Individual Trees by Intensity and Structure Features Derived from Airborne Laser Scanner Data." Remote Sensing of Environment 113 (6). Elsevier Inc.: 1163–1174. doi:10.1016/j.rse.2009.02.002.

Östberg, Johan, Tim Delshammar, Björn Wiström, and Anders Busse Nielsen. 2013. "Grading of Parameters for Urban Tree Inventories by City Officials, Arborists, and Academics Using the Delphi Method." Environmental Management 51 (3): 694–708. doi:10.1007/s00267-012-9973-8.

PCI Geomatics. 2015. ATCOR Ground Reflectance Workflow. http://www.pcigeomatics.com/pdf/geomatica/tutorials/Geomatica_2015_ATCOR.pdf

PCI Geomatics. 2018. TEX Texture Analysis. http://www.pcigeomatics.com/geomatica-help/references/pciFunction_r/python/P_tex.html

Pu, Ruiliang. 2017. Hyperspectral Remote Sensing. Boca Raton : Taylor & Francis: CRC Press. doi:10.1201/9781315120607.

Rodríguez, Juan Diego, Aritz Pérez, and Jose Antonio Lozano. 2010. "Sensitivity Analysis of K-Fold Cross Validation in Prediction Error Estimation." IEEE Transactions on Pattern Analysis and Machine Intelligence 32 (3). IEEE: 569–575. doi:10.1109/TPAMI.2009.187.

Shang, X, and LA Chisholm. 2014. "Classification of Australian Native Forest Species Using Hyperspectral Remote Sensing and Machine-Learning Classification Algorithms." IEEE Journal of Selected Topics in Signal Processing 7 (6): 2481–2489. http://ieeexplore.ieee.org/xpls/abs_all.jsp?arnumber=6626350.

Shen, Xin, and Lin Cao. 2017. "Tree-Species Classification in Subtropical Forests Using Airborne Hyperspectral and LiDAR Data." Remote Sensing 9 (11). doi:10.3390/rs9111180.

Shi, Yifang, Tiejun Wang, Andrew K. Skidmore, and Marco Heurich. 2018. "Important LiDAR Metrics for Discriminating Forest Tree Species in Central Europe." ISPRS Journal of Photogrammetry and Remote Sensing 137. International Society for Photogrammetry and Remote Sensing, Inc. (ISPRS): 163–174. doi:10.1016/j.isprsjprs.2018.02.002.

Transson, Julie, Raphaël d'Andrimont, Alexandre Maugnard, and Pierre Defourny. 2018. "Survey of Hyperspectral Earth Observation Applications from Space in the Sentinel-2 Context." Remote Sensing 10 (2): 1–32. doi:10.3390/rs10020157.

Vaughn, Nicholas R., L. Monika Moskal, and Eric C. Turnblom. 2012. "Tree Species Detection Accuracies Using Discrete Point Lidar and Airborne Waveform Lidar." Remote Sensing 4 (2): 377–403. doi:10.3390/rs4020377.

Zhang, Caiyun, and Fang Qiu. 2012. "Mapping Individual Tree Species in an Urban Forest Using Airborne Lidar Data and Hyperspectral Imagery." Photogrammetric Engineering & Remote Sensing 78 (10): 1079–1087. doi:10.14358/PERS.78.10.1079.

Chapter 3

3 Classification of Vegetation Using Multitemporal Planetscope and VENuS Imagery

3.1 Introduction

The classification of vegetation in imagery can be improved by making use of phenology. Phenology is the predictable, seasonal development of natural ecosystems, including vegetation (Jensen 2005). In remote sensing, more focus is given to seasonal patterns of vegetation, rather than specific events in vegetation development such as bud burst. Metrics relating to phenology have been calculated from remote sensing data, such as USGS Remote Sensing Phenology Products. A more common use is to utilize phenological information already present in the image to classify vegetation (Schwartz 2013).

Different types of vegetation differ in the timing of their phenological stages. This affects the spectral reflectance of vegetation and can aid in identifying them in imagery (Jensen 2005). Images taken at different dates can capture changing vegetation phenology. The additional phenological information provided by including images from multiple dates can make up for lower spectral resolution (Tigges, Lakes, and Hostert 2013). Past studies have generally found an improvement in classification accuracy when multiple image dates are used, although the degree of improvement varies. For example, Tigges et al. 2013 made use of five Rapideye images to classify stands of trees of the same genus. Compared to using a single image, multidate imagery improved the kappa by 0.31. In contrast, Richter et al. 2016 made use of hyperspectral imagery from two dates to classify ten species and found a small increase to accuracy of 4 percentage points when using both image dates rather than a single image (Table 3.1). Multidate classification is also beneficial when classifying broader land cover groups. A classification of land cover in Chile improved accuracy between 5-10 percentage points (with greater increases for simpler classification schemes) when using four-season imagery (Zhao et al. 2016). The classification scheme differentiating conifer and deciduous forest resulted in an increase of 8 percentage points to overall accuracy. Xie et

al. 2019 classified several species of trees, as well as other land cover, and increased accuracy by 7.77 percentage points using bitemporal classification.

Table 3.1: Past studies that used multidate imagery to classify tree species or vegetation cover.

Year/ Author	Sensor	Resol- ution (m)	Number Of Dates	Classifier	Number of Classes	Features Classified	Overall Accuracy	Increase From Single Date
2010 Hill	Airborne Thematic Mapper	2	3	MLC	6	Tree Genera	88.00%	17.40
2013 Tigges	RapidEye	5	5	SVM	8	Tree Genera	0.83 kappa	0.31 kappa
2015 Li	Worldview 2/3	0.5	2	SVM	5	Tree Species	92.40%	9.70
2016 Richter	AISA Dual	2	2	PLS-DA	10	Tree Species	78.40%	3.80
2016 Zhao	Landsat 8 OLI	30	4	RF	10/30/35	Land Cover	80/73/59%	10/8/5
2017 Le Louarn	Pleiades	0.5	2	RF	6	Tree Species	79.20%	13.90
2019 Xie	ZiYuan-3	2	2	MLC	13	Tree Species/ Land Cover	76.39%	7.77

The ability of multiple dates to improve classification is clear, but it is also important to consider the exact dates of images, as the dates when trees are most distinguishable can vary. For example, Hill et al. 2010 noted that trees would have been better differentiated if an image from April had been included to capture the first appearance of leaves and buds. Past studies have indicated that spectral differences between trees are greater early in the growing season than in summer (Tigges, Lakes, and Hostert 2013). Zhao et al. 2016 also found better results from the date corresponding to the growing season when classifying land cover.

This study focused on assessing the ability of two multispectral sensors with high spatial and temporal resolution, Planetscope and VENuS, to classify vegetation. Both sensors are new and have rarely been used for vegetation classification. However, their high revisit times make them well suited for multitemporal classification. The goals of the study were:

1) Accurately classify the study area into deciduous trees, conifers, non-tree vegetation and non-vegetation using Planetscope and VENuS images.

2) Determine which time of the year is best for differentiating these classes.

3) Assess whether using multiple image dates improves classification accuracy over using single dates.

4) Compare the classification accuracy between Planetscope (higher spatial resolution, lower spectral resolution) and VENuS (higher spectral resolution, lower spatial resolution).

3.2   Methodology

3.2.1   Study Area

The study area covers 56.58 km^2 in the west of London, Ontario (Figure 3.1).
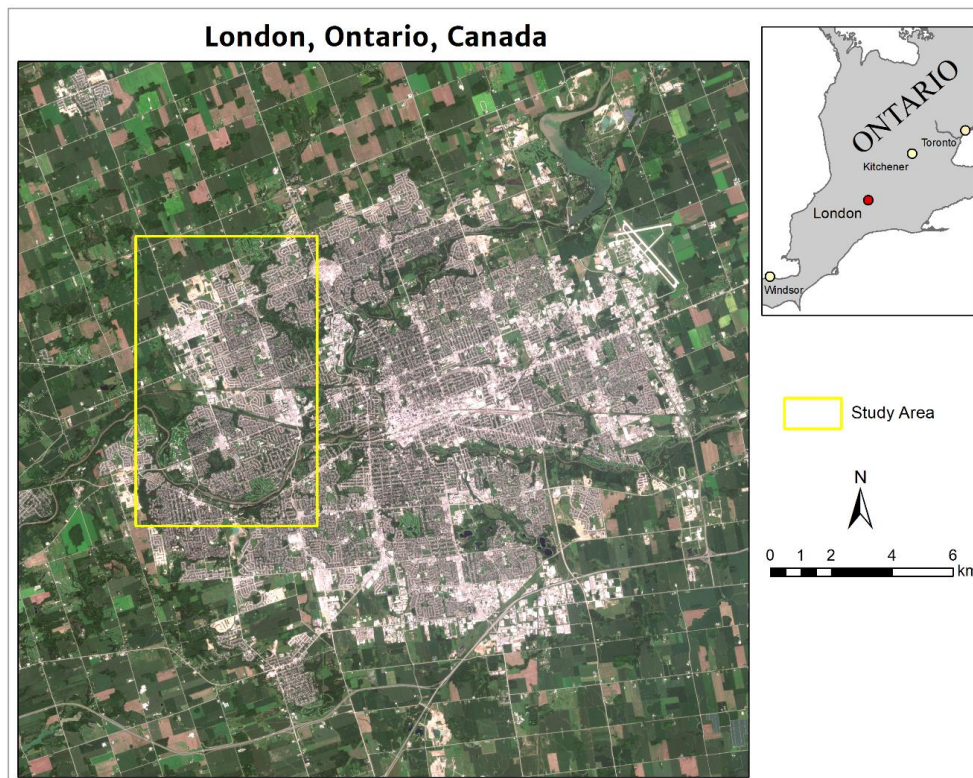
Figure 3.1: Location of study area (yellow) within London, Ontario.

The land cover within this area is diverse, with trees growing in different settings. Residential areas contain trees mixed in with buildings, roads and lawns. Parks and golf courses contain both isolated and clustered trees, as well as large areas of grass. Agricultural land outside the city contains dense woodlots, as well as isolated trees in fields alongside crops. The study area also contains woodlands with large numbers of trees. This includes three environmentally significant areas: Medway Creek, Sifton Bog, and Warbler Woods. London is located in the Carolinian zone of Canada, the only primarily deciduous forest in Canada (Drushka 2003). As such, broadleaf deciduous species represent the majority of trees in the study area. However, Sifton Bog is an anomaly, containing black spruce and tamarack which are more common in Northern Ontario. Tamarack is distinct as it is a deciduous conifer. Additionally, conifers planted by humans can be found both in wooded areas, as well as in residential areas. The diversity of tree locations and their influences is further discussed in this paper.

3.2.2 Data Description

Imagery was obtained from two satellite sensors: VENuS and Planetscope. VENuS (Vegetation and Environment monitoring on a New MicroSatellite) was developed jointly by the Israeli Space Agency and the French National Centre for Space Studies. It travels in sun-synchronous orbit at an altitude of 720 km and completes and orbits the earth 29 times every two days. Planetscope is operated by the Planet Labs company. It is not a single satellite but rather a constellation of over 120 miniature Dove satellites which are in sun-synchronous orbit at an altitude of 475 km. The constellation orbits the earth's poles every 90 minutes. Both sensors are well suited to multidate classification because of their frequent revisit times. VENuS captures the same location every two days, while Planetscope revisits daily, although at the time of writing imagery does not appear to be available at this frequency. Nonetheless, there are many images available, so it was possible to obtain clear images for all seasons. Planetscope has 3 m spatial resolution, which is higher than VENuS which is 5 m. Planetscope is more limited in spectral resolution with only four bands, while VENuS has 12 (although two cover the same wavelength ranges) (Table 3.2).

Table 3.2: Spectral bands of Planetscope and VENuS sensors.

	Planetscope			VENuS		
	Wavelength (nm)	Colour	Spatial Resolution	Wavelength (nm)	Colour	Spatial Resolution
Band 1	455 - 515	Blue	3 m	395 - 435	Blue	5 m
Band 2	500 - 590	Green	3 m	420 -460	Blue	5 m
Band 3	590 - 670	Red	3 m	470 - 519	Blue-Green	5 m
Band 4	780 - 860	Near Infrared	3 m	535 - 575	Green	5 m
Band 5				600 - 640	Red	5 m
Band 6				600 - 640	Red	5 m
Band 7				652 - 682	Red Edge	5 m
Band 8				690 - 714	Red Edge	5 m
Band 9				734 - 750	Red Edge	5 m
Band 10				774 - 790	Red Edge	5 m
Band 11				845 - 885	Near Infrared	5 m
Band 12				900- 930	Near Infrared	5 m

Planetscope data was made available through the Planet education and research program. It is provided georeferenced, orthorectified and atmospherically corrected. VENuS is currently available only for select locations, one of which includes western London, Ontario. VENuS is also provided georeferenced and orthorectified. Atmospherically corrected surface reflectance is available at 10 m spatial resolution, however that was too coarse to meet the needs to the study. Instead, 5 m top-of-atmosphere reflectance products were used. The dates chosen were mostly free of cloud

and haze and focused on a fairly small area so this level of correction should be acceptable.

Four dates were chosen for Planetscope (Figure 3.2) and VENuS (Figure 3.3), representing different stages of leaf growth. The April images capture the study area before leaf growth has begun on trees. The May images have partial leaf growth, with leaves at different stages of development. July represents full leaf development. In October, leaves have begun to change colour and fall. For both April and July, images from the same date were available for both sensors. However, there was no clear May image in 2018 for VENuS, so a 2019 image was selected instead. This should be acceptable, as phenology is similar for the same time each year (Jensen 2005). However, exact timing differs due to factors such as weather, so the extent of leaf growth may differ between them (Li et al. 2015). The October Planetscope image is slightly later in the month than the VENuS image, with more changed and fallen leaves. The choice of dates was based on the suggestions in the literature that an image of full leaf growth should be combined with images from early leaf growth in spring, or senescence in autumn (Hill et al. 2010) (Tigges, Lakes, and Hostert 2013). However, the primary focus of this study is distinguishing coniferous and deciduous trees. April was included to have a date with no leaves on deciduous trees, to better distinguish them from conifers.

April 22, 2018   May 13, 2018

July 7, 2018   October 22, 2018
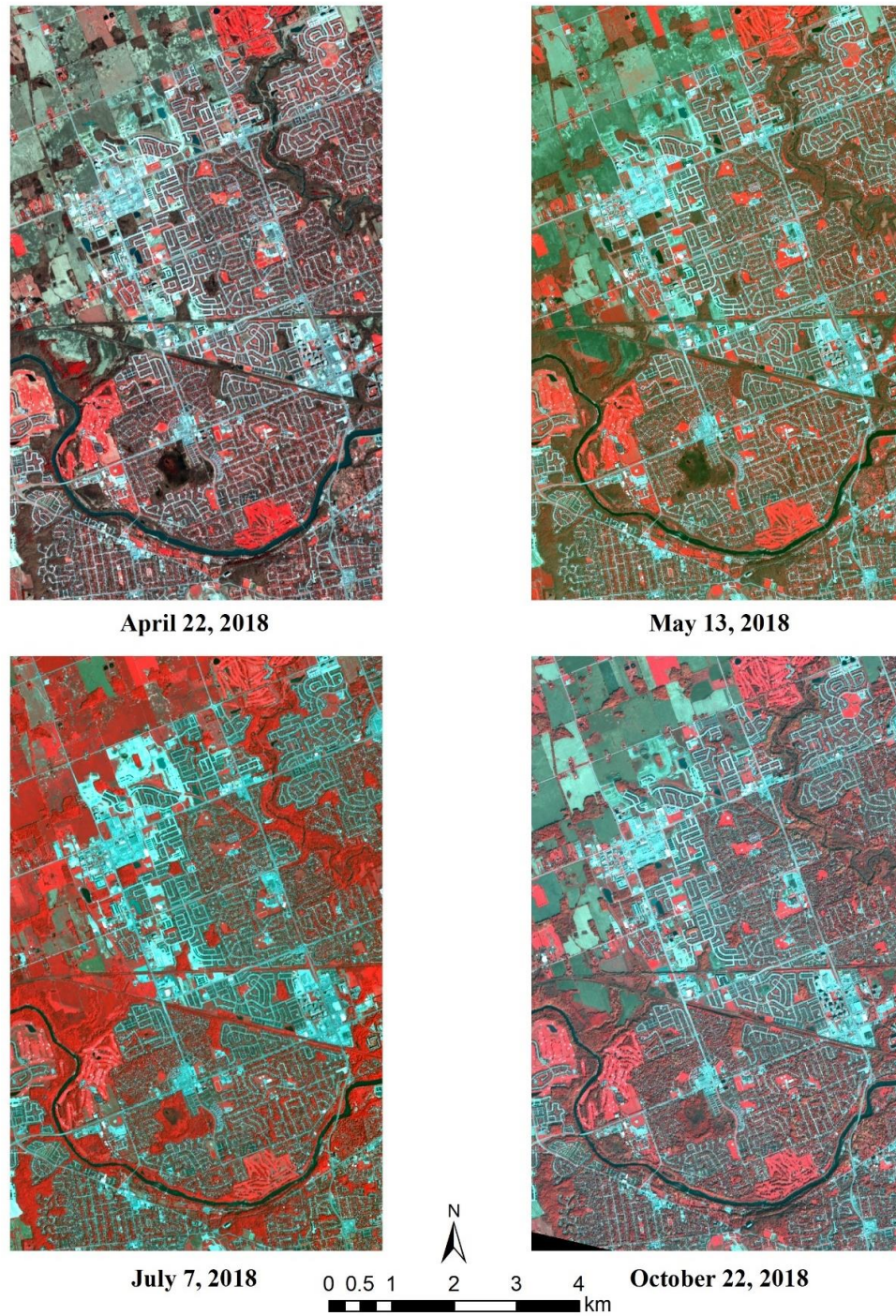
Figure 3.2: Planetscope images used for classification.

April 22, 2018   **May 15, 2019**

July 7, 2018   **October 9, 2018**
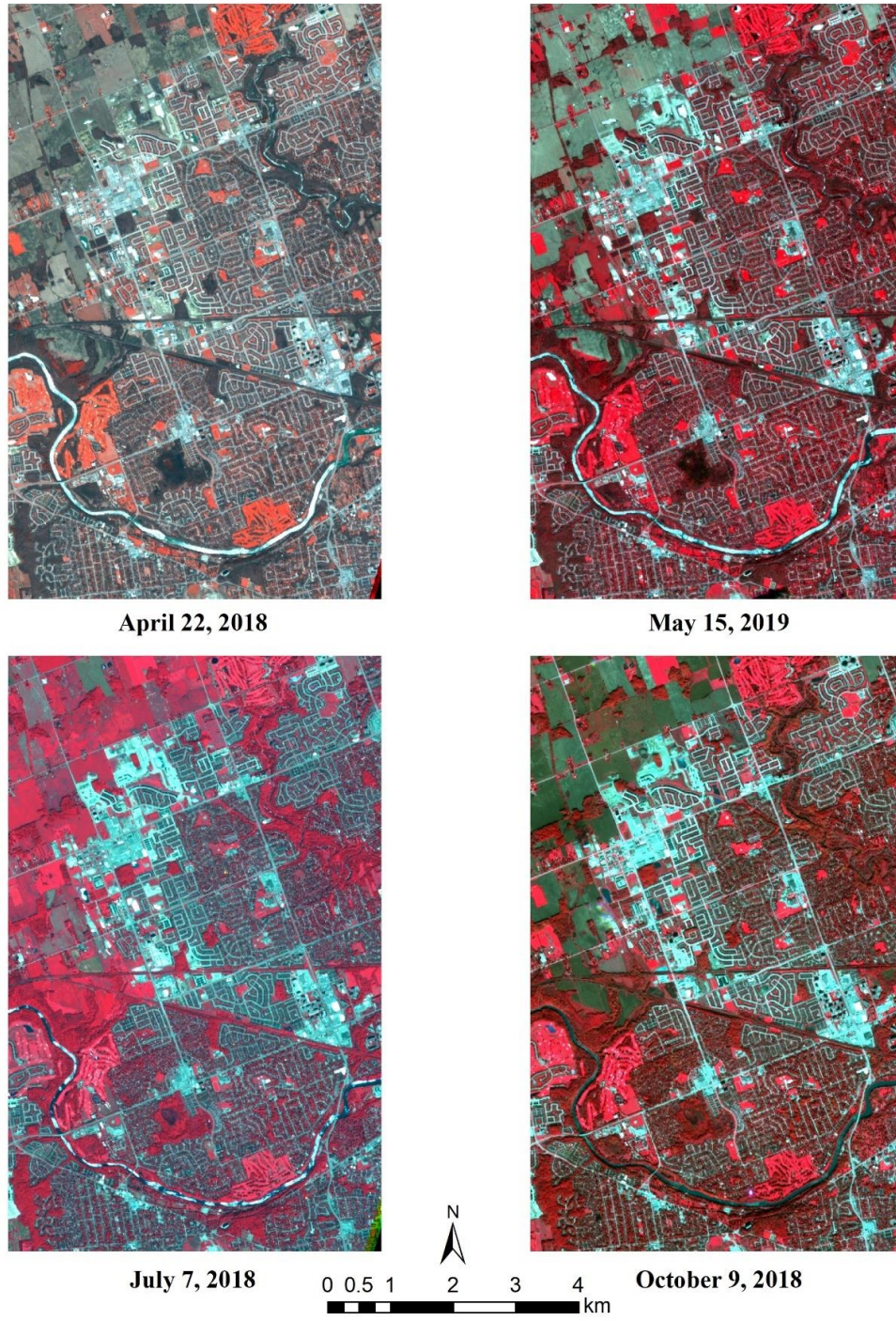
Figure 3.3: VENuS images used for classification.

3.2.3 Classification Process

Four classes were chosen to represent the study area. Trees were divided into deciduous and coniferous. Distinguishing between them was the primary goal of the study. All other vegetation was included in a non-tree vegetation class. In previous studies, other vegetation has more often been confused with trees. For example, grass was more often misclassified as tree than impervious surfaces or bare land in Xie et al. 2019, with a similar finding in Zhao et al. 2016. Therefore, it was of interest to analyze this as a distinct class. Finally, all non-vegetated land cover was grouped together. As spectral reflectance of vegetation differs greatly from other types of land cover, it was assumed that there would be little confusion with trees.

Areas were manually selected to act as training data for the classifier. Multiple training classes for each of the four classes were selected to account for spatial heterogeneity within classes (Table 3.3).

Table 3.3: Training classes used as input to classifier, and corresponding four final classes (Deciduous trees, coniferous trees, other vegetation, non-vegetation)

Deciduous Trees		Other Vegetation
Deciduous Forest		Bog
Deciduous Street		Grass
Maple/Beech Forest		Long Grass
Sugar Maple Forest		Low Vegetation
Deciduous Backyard		Grass Backyard
Deciduous Backyard Small		Crops
Deciduous Thicket/Shrub		
Coniferous Trees		**Non-Vegetation**
Conifer Forest		House
Conifer Various		Large Building
Conifer Backyard		Road
Conifer Backyard Small		Bare Earth
Tamarack/Spruce		Water

Among deciduous trees, classes were created for trees within dense clusters, along streets, and inside backyards. Drawing on a report on Medway Creek, classes were also created for areas identified as primarily sugar maple, and maple and beech forest (City of London). Thicket, representing small trees and shrubs, was also trained separately. Conifers had classes for dense clusters, and backyards. Additionally, a class was created for the tamarack and spruce forest present in the Sifton Bog. Tamarack is a deciduous conifer, shedding needles in winter. In the final classification, it was included as coniferous. Non-tree vegetation classes included grass (both in open areas and in backyards), crops, wild meadow (long grasses and low vegetation) and bog moss. Non-vegetation represented numerous classes including houses, concrete buildings, roads, water and bare earth. Higher resolution imagery and a normalized digital surface model (representing heights of objects in the study area) were used to aid in determining land cover when selecting training sites. Maps of land cover in the environmentally significant areas of London (including Medway Creek, Sifton Bog and Warbler Woods) were provided by the Upper Thames Conservation Authority.

Following training area creation, classification was carried out in ENVI using support vector machine classification (SVM). SVM is a machine learning classifier that finds the hyperplane that best separates two groups of data. For groups that are not linearly separable, the data can be transformed into a higher dimension using a kernel function, which allows for better classification. SVM was originally a binary classifier, but it can be modified to allow classification of multiple classes (Pu 2017). In the case of ENVI, classification is carried out for each pixel in the image (Harris Geospatial). With Planetscope all four bands were used as features for the classifier, while for VENuS band 6 was excluded as it covers the same wavelength range as band 5. SVM performs better when the parameters are tuned to data being classified. However, the long processing time for classification made this impractical, so the default parameters were used instead. This included making use of the radial basis function kernel. Accuracy assessment was carried out following classification.

Classification accuracy was assessed through the use of randomly generated points. The true land cover for each point was determined, after which it was compared to

the class of the pixel it falls on in the classified images. These were stratified based on the results of the four-date Planetscope classification to the percentage of each of the four classes in the image. 600 points were generated, of which 586 were used, with some excluded as it was too difficult to determine the land cover present.

Based on the difference between real-world class and the classification result for each point, a confusion matrix was constructed. This shows the class each point actually belongs to, and what it was classified as. From the matrix, producer's and user's accuracies can be calculated for each class. Producer's accuracy is based on the columns of the table and indicates the probability that a pixel belonging to a class based on real world reference data was correctly assigned to that class. User's accuracy is based on the rows and indicates the probability that a pixel assigned to a certain class by the classifier truly belong to that class. Overall accuracy is based on the diagonal cells in the matrix and indicates what percentage of points were correctly classified (Lillesand, Kiefer, and Chipman 2008). Another measure of accuracy, kappa, is also generated. Kappa takes into account chance agreement, based on the row and column totals of the confusion matrix (Jensen 2005). Following accuracy assessment, the results were analyzed.

3.3 Results

3.3.1 Overall Accuracy

Classification using Planetscope imagery always had higher accuracy than classification using VENuS imagery, although the extent varied (Table 3.4). Overall accuracy when using single date images was similar between Planetscope and VENuS. For both sensors, April performed best, followed by May then October, while July imagery produced the least accurate classification. With single date classification, Planetscope outperformed VENuS most when using in April and July images, while there was little difference when using May and October images.

Table 3.4: Overall accuracy and kappa of classification results, for all combinations of dates.

Image Dates	Planetscope Overall Accuracy	VENuS Overall Accuracy	Planetscope Kappa	VENuS Kappa
Four date	83.11%	70.99%	0.76	0.58
April	74.92%	70.65%	0.63	0.57
May	71.50%	69.97%	0.58	0.56
July	67.07%	61.26%	0.54	0.47
October	68.26%	67.58%	0.53	0.53
April + July	83.11%	71.84%	0.76	0.60
May + July	81.23%	72.18%	0.73	0.60
October + July	79.52%	69.28%	0.71	0.57

Planetscope more clearly outperformed VENuS when using multidate classification. Four-date classification with Planetscope was 12.12 percentage points higher than four-date classification with VENuS, and 10.92 percentage points higher than the best (two-date May/July) VENuS result. The results with two-date classification were similar, with Planetscope greatly outperforming VENuS. However, there was less of a difference between the two sensors when classification was performed with only one date. At the lowest, the Planetscope October classification was only 0.68 percentage points higher than the corresponding VENuS result.

For Planetscope, using multiple image dates clearly outperformed using only single dates. In all cases, combining the July image with another date results in higher accuracy than either alone. When combined with July imagery, accuracy was highest for April, followed by May then October. This is the same ranking as when using single dates. However, the least accurate two-date classification (July/October) still performed better than the best single date classification (April). Overall, the best multidate Planetscope classification (all four dates combined) had an overall accuracy 8.19 percentage points higher than the best single date classification (April). Overall accuracy when using only the two-date April/July classification and when using all four images was the same. Due to this result, no further combinations were tested (e.g. three-date classification) as using only two-dates already performed as well as using all four images. In contrast, there is less of a difference in accuracy between classification with single or

multiple VENuS images. The best multidate classifications (May/July, April/July) had slightly higher overall accuracy than the best single date classification (April), while the least accurate two-date classification (October/July) performed worse. Classification results using April/July, and May/July images had slightly higher overall accuracy than classification using all four dates.

3.3.2 Class Accuracy

Differences in accuracy between sensors and image combinations also appeared for individual classes (Table 3.5 and

Table 3.6). Confusion between classes also differs between date combinations, as seen in the confusion matrices (see Appendix C). Four-date Planetscope classification provided the best producer's accuracy for deciduous trees, while using two-date April/July images was marginally lower. VENuS was similar, with two-date April/July imagery best classifying deciduous trees, and four-date classification being slightly less accurate. For both sensors, confusion of deciduous species occurred primarily with non-tree vegetation. Planetscope also classified coniferous best using all four images. However, with VENuS four-date and April/July producer's accuracies were lower for coniferous, particularly four-date classification. Instead, October/July classification was more accurate. Confusion for conifers was more common with deciduous trees than non-tree vegetation with Planetscope, but evenly split with VENuS. When classifying non-tree vegetation, Planetscope May/July images performed best, followed by October/July and April/July. The best result for non-tree vegetation for VENuS was May/July images. Non-vegetation

was best classified by Planetscope October/July images, while the best classification from VENuS made use of only October imagery.

Producer's accuracy for deciduous trees was lowest in July for both sensors. Confusion occurred with conifers and other vegetation. Confusion was somewhat greater for other vegetation with Planetscope, and with conifers for VENuS. Conifers were classified least accurately in May and July with Planetscope, being confused mainly with deciduous trees. Conifer producer's accuracy was also low for the May image with VENuS, but four-date classification was the second lowest. Confusion occurred with both deciduous trees and other vegetation. Non-tree vegetation producer's accuracy was lowest with the October image for both sensors. Non-vegetation producer's accuracy was lowest in May for Planetscope, while with VENuS it was lowest when using two-date April/July imagery.

User's accuracy differed greatly from producer's accuracy in some cases. Non-vegetation was fairly stable with high values for both measures of accuracy. In contrast, deciduous and coniferous trees had some very different results. For example, the July classification was the least accurate Planetscope date for deciduous trees based on producer's accuracy, but the most accurate based on user's accuracy. There were also some cases where VENuS user's accuracy outperformed Planetscope. Large differences also existed for conifers, with user's accuracy almost always being lower than producer's accuracy. Results also differed for the same date when comparing user's and producer's accuracy. For example, Planetscope May/July and October/July classifications had the same producer's accuracy for conifers, but May/July user's accuracy was higher. July was the highest single VENuS date for conifers according to producer's accuracy, but the lowest according to user's accuracy. Four-date classification using Planetscope had high or highest values for both measures of accuracy.

Table 3.5: Producer's accuracy for each class, for all combinations of dates.

Deciduous Producer's Accuracy					Other Vegetation Producer's Accuracy				
Planetscope			VENuS		Planetscope			VENuS	
Four date	74.56%		Four date	66.67%	Four date	82.58%		Four date	73.75%
April	63.31%		April	53.57%	April	79.28%		April	78.45%
May	57.40%		May	51.79%	May	81.51%		May	78.51%
July	20.12%		July	33.93%	July	79.86%		July	75.84%
October	38.46%		October	41.67%	October	76.32%		October	70.00%
April + July	73.96%		April + July	67.26%	April + July	84.31%		April + July	79.62%
May + July	69.23%		May + July	61.31%	May + July	87.66%		May + July	82.91%
October + July	56.80%		October + July	48.81%	October + July	85.62%		October + July	82.17%

Conifer Producer's Accuracy					Non-Vegetation Producer's Accuracy				
Planetscope			VENuS		Planetscope			VENuS	
Four date	73.33%		Four date	43.33%	Four date	90.95%		Four date	75.88%
April	60.00%		April	50.00%	April	81.88%		April	80.15%
May	43.33%		May	40.00%	May	79.10%		May	80.90%
July	53.33%		July	53.33%	July	93.83%		July	72.38%
October	43.33%		October	50.00%	October	86.08%		October	84.70%
April + July	66.67%		April + July	53.33%	April + July	91.03%		April + July	72.29%
May + July	60.00%		May + July	46.67%	May + July	88.41%		May + July	76.09%
October + July	60.00%		October + July	63.33%	October + July	94.44%		October + July	76.19%

Table 3.6: User's accuracy for each class, for all combinations of dates.

Deciduous User's Accuracy						Other Vegetation User's Accuracy					
Planetscope			VENuS			Planetscope			VENuS		
Four date	85.14%		Four date	76.71%		Four date	71.51%		Four date	57.28%	
April	76.98%		April	82.57%		April	55.70%		April	48.92%	
May	75.19%		May	80.56%		May	52.43%		May	48.72%	
July	94.44%		July	77.03%		July	53.00%		July	51.60%	
October	66.33%		October	79.55%		October	55.06%		October	50.00%	
April + July	85.03%		April + July	84.96%		April + July	71.67%		April + July	56.56%	
May + July	85.40%		May + July	82.40%		May + July	70.31%		May + July	57.71%	
October + July	88.07%		October + July	80.39%		October + July	72.38%		October + July	60.28%	
Conifer User's Accuracy						Non-Vegetation User's Accuracy					
Planetscope			VENuS			Planetscope			VENuS		
Four date	61.11%		Four date	38.24%		Four date	94.62%		Four date	86.50%	
April	58.06%		April	48.39%		April	87.60%		April	83.85%	
May	37.14%		May	50.00%		May	89.45%		May	83.40%	
July	19.05%		July	16.00%		July	91.57%		July	89.64%	
October	20.97%		October	22.39%		October	87.69%		October	86.31%	
April + July	58.82%		April + July	39.02%		April + July	94.67%		April + July	87.43%	
May + July	40.00%		May + July	34.15%		May + July	97.17%		May + July	90.67%	
October + July	29.03%		October + July	25.00%		October + July	94.44%		October + July	90.72%	

3.3.3 Spectral Plots

Confusion between classes is due to similar spectral reflectance. The spectral response of training classes varied throughout the year, as can be seen by examining the spectral profiles of Planetscope (Figure 3.4) and VENuS (Figure 3.5).
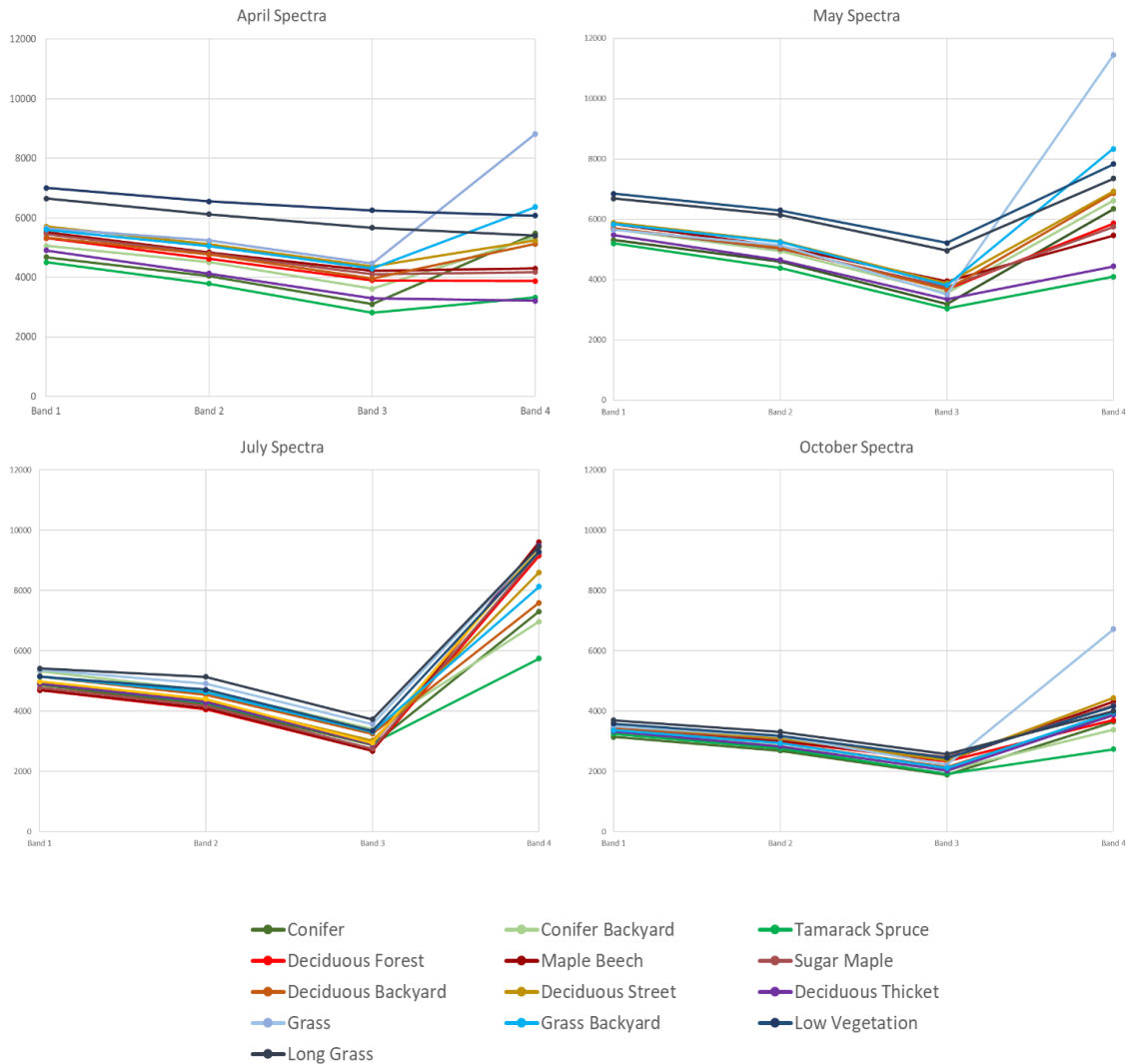
Figure 3.4: Planetscope spectral means for vegetation training classes.
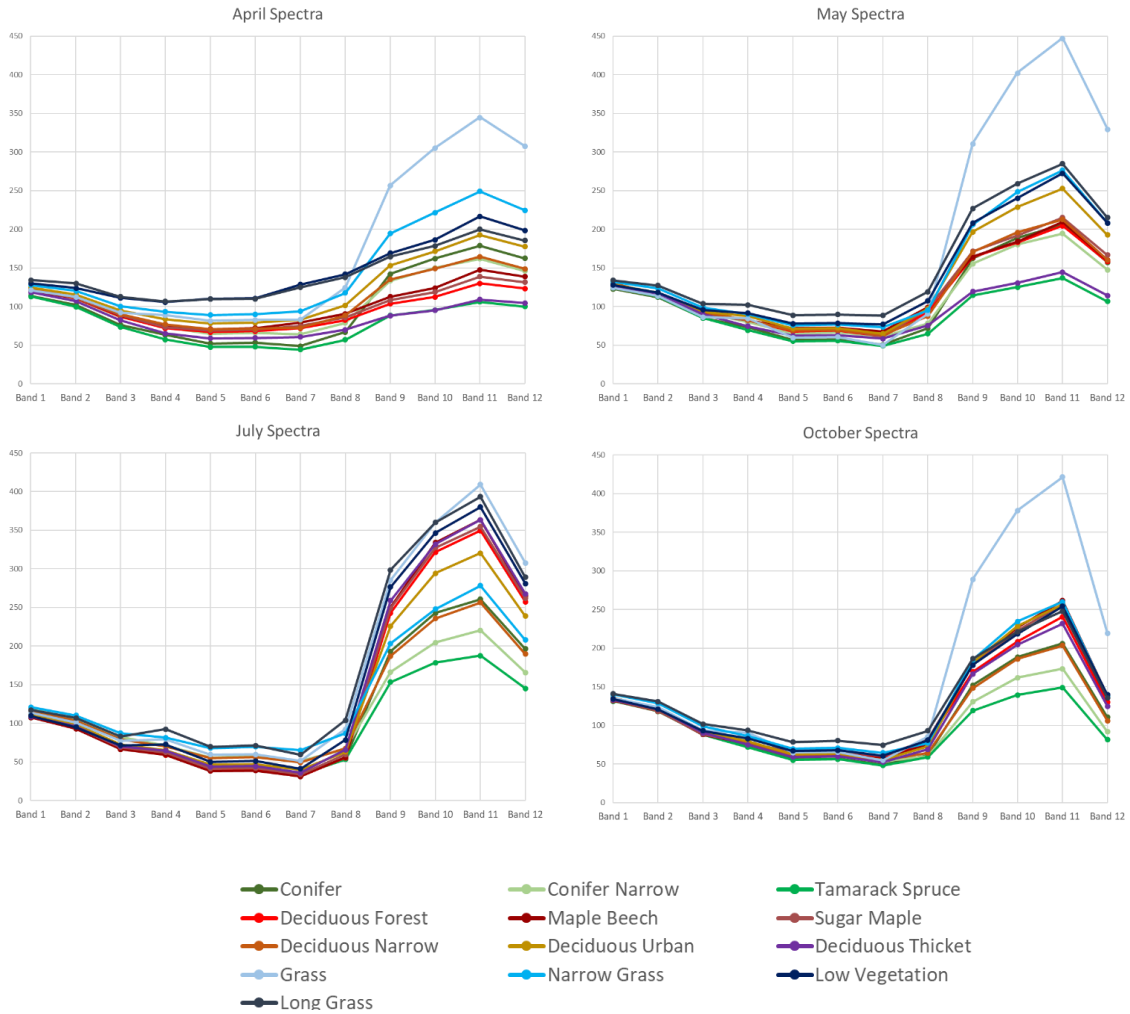
Figure 3.5: VENuS spectral means for vegetation training classes.

July had the lowest overall accuracy for both sensors, and also noticeable similarities between the spectral profiles of different classes. In the Planetscope image, many of the classes cluster together, with similar spectral means. This is particularly true for forest deciduous trees and non-tree vegetation. Deciduous and conifers in narrow areas also have similar reflectance. With VENuS, spectral means are similar for most classes in blue to red edge bands, with the exception of grasses. Tamarack/spruce and narrow conifer are fairly distinct from other classes in the NIR range, but the main conifer class is very similar to narrow deciduous. Deciduous classes and non-tree vegetation are somewhat separable in the red edge and NIR ranges.

The Planetscope April image had the highest producer's accuracy among single-date classification for both deciduous and coniferous trees. Most classes have a distinct spectral curve, although in specific bands certain training classes from different vegetation types are similar (e.g. urban and narrow deciduous, and crops in NIR band). NIR for conifers is higher than for deciduous, as is expected because this image is before leaf growth for deciduous trees. Surprisingly, conifers are still lower in green reflectance than deciduous trees. This could potentially be due to undergrowth or grass below deciduous trees. In the April VENuS image, deciduous forest trees are distinct, but narrow conifer and deciduous training classes have very similar reflectance. As with Planetscope, conifer reflectance is low for most bands including green, but rises sharply in the NIR bands.

In May, the spectral curves of different classes are more similar than in April, but not as close as July. Although they mostly follow the typical vegetation reflectance trend, the actual values are distinct. Tamarack and deciduous thicket both still have low NIR reflectance, indicating that they may grow foliage later than the other training classes. Most coniferous and deciduous tree classes have similar reflectance. This seems to match the high confusion of conifers with deciduous. However, deciduous was more often misclassified as other vegetation. The agricultural crop training class is the only one to have similar reflectance to deciduous tree classes. The VENuS May image is similar, with all classes following the typical vegetation curve, and similar reflectance curves being present for both conifers and deciduous. Compared to other dates, the curves of conifers closely followed those of deciduous trees.

The October image for Planetscope also follows typical vegetation reflectance curves, with the exact values being closer than in May and similar to July. Deciduous trees were most often misclassified as conifers in October, although the reason is not apparent from the reflectance curves, with conifers and grasses both being differing from deciduous training classes to a similar degree. For VENuS, most training classes follow a similar trend, and exact spectral means appear very similar for this date. For both sensors, there is a decline in NIR reflectance for most classes compared to summer, with the exception of grass which remains high.

3.3.4 Map Analysis

Differences between classification results using different sensors and dates also appeared when examining the maps produced through pixel classification (Figure 3.6 and Figure 3.7.

Figure 3.6: Classification result using four-date Planetscope imagery

Figure 3.7: Classification result using four-date VENuS imagery

When examining the four-date classification using Planetscope and VENuS, distinct differences appeared in several areas. In the Medway Valley, the creek was somewhat more prominent in the VENuS classification, as was non-tree vegetation. VENuS generally had more homogenous areas, due to the larger pixel size. This was also noticeable in the neighbourhood north of the creek, with non-tree vegetation covering areas that were distinguished as tree in the Planetscope classification (Figure 3.8). In most residential areas, Planetscope seemed to classify too many pixels as non-vegetation while VENuS did not classify enough and missed smaller buildings. In newer neighbourhoods with smaller trees, Planetscope classified trees that VENuS missed (Figure 3.9). Broadly though, the two classifications were very similar visually.
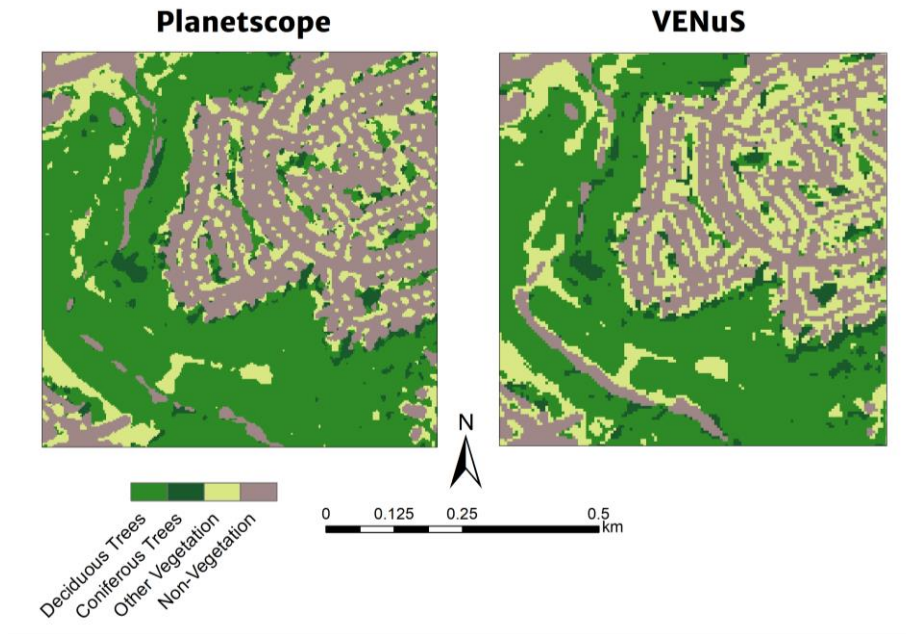
Figure 3.8: Medway Creek and surrounding neighbourhood in four-date Planetscope and VENuS classifications
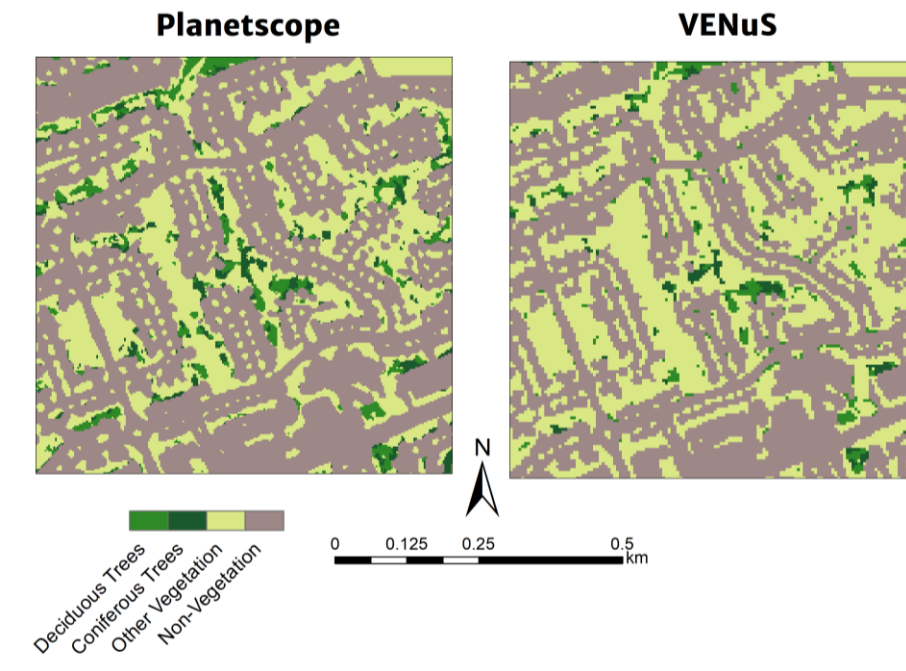
Figure 3.9: Four-date Planetscope and VENuS classifications of relatively new subdivision in North London, containing mostly small trees

Examining the different image date classification results showed clearer differences for Planetscope (see Appendix D, Figures D-1 to D-7). Planetscope April classification was similar to four-date classification in most ways. Some differences included creeks and rivers appearing more clearly, due to the lack of overhanging leaves, and some forested areas being misclassified as non-tree vegetation. May also had relatively less vegetation, and had many forested areas incorrectly identified as coniferous. July had the most noticeable problems, with many forested areas classified as non-tree vegetation. The confusion between tree and non-tree vegetation classes was very noticeable visually for this date. This confusion was also noticeable in the October classification. Two-date classifications differed less when compared to four-date classification. April/July classification, which had comparable overall accuracy, had somewhat more non-tree vegetation at the expense of non-vegetation and trees. In several rural areas, this appeared to be the correct classification. May/July had similar issues as May, incorrectly classifying many trees as coniferous. October/July classification incorrectly classified Medway Creek as coniferous trees.

Comparing four-date VENuS classification to other results also showed differences (see Appendix D, Figures D-7 to D-14). April classification for VENuS was similar to April Planetscope results, with more pixels identified as non-tree rather than tree, and Medway Creek clearly classified. May classification also had somewhat fewer tree pixels but did not differ greatly from the four-date image. July classification had noticeable areas of non-tree vegetation being classified as trees, and too many pixels identified as conifers. Over-classification of conifers was even more noticeable in the October image. The differences between four-date and two-date classification with VENuS were not particularly notable.

3.4 Discussion

Classification accuracy was affected by location, with pixels in more homogenous areas being better classified. For Planetscope four-date classification, deciduous tree accuracy was 91.94% in heavily forested areas but 64.49% outside of them. VENuS four-date classification accuracy for deciduous trees was 95.16% within densely wooded areas and 50% outside. For other classes, the number within forested areas is too small to draw

conclusions. This is due to the spatial resolution of the sensors. The 3 and 5 m pixel sizes of Planetscope and VENuS, respectively, make it difficult to correctly classify trees surrounded by other land cover. Pixels containing the tree crown likely also contain spectra from surrounding features such as grass, roads or buildings. This affects the spectral response of the pixel, sometimes enough to no longer clearly belong to its proper class. Changing foliage in clusters of deciduous trees is clearly detected, with a moderate change in green reflectance and a large decrease in NDVI reflectance. However, there is less change to pixel values for many trees along residential streets. These trees are surrounded by grass so during periods without leaves, the pixel value may be influenced by reflectance off of grass visible through the bare branches. In April, grass already has fairly high reflectance in green and NIR, while deciduous trees are characterized by lower values in these wavelength ranges during that time. Trees also overhang roads and buildings, so that there are many mixed pixels representing reflectance from trees and man-made structures. All of this contributes to the lower accuracy of trees within more built-up areas.

The spatial resolution of the imagery also causes issues for assessing classification accuracy. The georeferencing of Planetscope and VENuS images is not perfect, so it can be difficult to determine the exact location of the pixel being assessed in the reference data. It is possible that an accuracy assessment point on the edge of a tree, according to higher resolution data sources, may actually be outside of the tree entirely in the Planetscope or VENuS image. At the resolution of these sensors, it is difficult to differentiate isolated trees from other vegetation. There are presumably errors within accuracy assessment because of this, which may lead to lower accuracy values.

Other issues in classification can be attributed to training classes. Several improvements should have been made to better distinguish types of vegetation. In October certain trees had lost leaves, other changed colour, and others had little change from summer. In May, leaf growth was at different stages for different trees. Further dividing deciduous training classes by taking into account which areas experienced these phenological stages could have improved classification. The same is true of agricultural fields. While these were changed for each single-date to ensure bare fields were not

included as training for crops, a single training class was used for the four-date classification. This included any field that had crops in any of the four images. It would have been better to have multiple crop training classes, based on which images had crops present. The overly general training classes may explain some of the confusion between vegetation and non-vegetation.

It is not clear from the spectral plots why accuracy substantially improved when combining multiple dates for Planetscope but did not for VENuS. Differences between dates are somewhat more pronounced for Planetscope. This is especially true of April, where the relatively lower NIR reflectance compared to other dates is more notable with Planetscope than it is with VENuS. However, the differences between dates still appear in VENuS. It may simply be due to the lower spatial resolution of VENuS. Training samples, with the exception of the backyard classes, were selected in areas where a given class was clearly distinguishable. However, the low resolution of VENuS resulted in more mixed pixels, which would not share the spectral signatures of these purer classes. Therefore, the changes to reflectance over the seasons for purer training classes may not closely match the same land cover in areas with more mixed pixels.

The higher accuracy of Planetscope for all tested image date combinations suggests that spatial resolution was more important that spectral resolution. The higher accuracy of VENuS within dense forest, where large homogenous areas make spatial resolution less important, show that spectral resolution is a benefit to classification. However, when classifying urban trees those uniform stands of trees are relatively rare. A past study using higher resolution imagery obtained similar overall accuracy classifying trees in an urban area, while identifying four specific species in addition to general broadleaf and conifer classes (Le Louarn et al. 2017). This was accomplished using a sensor with 0.5 m spatial resolution and using only two dates. However, both Planetscope and VENuS have a benefit over higher resolution sensors because their data is more easily obtainable. This is due to the high revisit frequency, as well as programs that provide free imagery for academic purposes. Even when purchased, Planetscope is more affordable than high resolution sensors such as Pleiades and Worldview (Sozzi et al. 2018).

The results are generally lower when compared to past studies. Tigges, Lakes, and Hostert 2013 classified the one coniferous species in their study with near perfect accuracy. Non-tree pixels were masked out and not accounted for, nor were other species of conifers. Conifers were also perfectly classified in Le Louarn et al. 2017 when using bitemporal classification. The three conifers in Sheeren et al. 2016 had over 90% accuracy and were misclassified most commonly with the other conifer classes. In contrast, the accuracy of coniferous and deciduous trees in this study was only similar to the forest class in Zhao et al. 2016. This study differed from Tigges, Lakes, and Hostert 2013 and Sheeren et al. 2016 due to their use of homogenous areas greater than one pixel for training and testing. Thus, the issue of mixed pixels did not influence their studies. Le Louarn et al. 2017 made use of a higher resolution sensor (Pleiades pansharpened to 0.5 m spatial resolution) and used object-based classification. Zhao et al. 2016 made use of coarser resolution Landsat, which at 30 m spatial resolution is larger than the size of individual trees.

In comparison to other studies, Planetscope behaved as expected, with higher accuracy when using multiple image dates for classification. The degree of improvement was similar to past studies. The low improvement of VENuS is unusual in comparison, with only Richter et al. 2016 having a similarly low increase with multitemporal classification. However, that study focused only on distinguishing between tree species and made use of hyperspectral data from two dates, so there is little similarity with the results of VENuS classification in this study.

3.5 Conclusions

This study made use of four images of different seasons from Planetscope and VENuS sensors in order to classify land cover in London, Ontario into deciduous trees, coniferous trees, non-tree vegetation and non-vegetation using support vector machine classification. The main results were:

1) 83.11% overall accuracy was achieved with four-date and two-date (April/July) Planetscope images, while 72.18% overall accuracy was reached with two-date (May/July) VENuS images.

2) April, before leaves had begun to grow on deciduous trees, was the best time for distinguishing these classes according to overall accuracy. It also provided the best producer's accuracy for conifer and deciduous classes when using Planetscope imagery, as well as a relatively high user's accuracy. April VENuS imagery also best classified deciduous and coniferous trees, when considering both user's and producer's accuracy.

3) Combining multiple dates substantially improved classification when using Planetscope imagery. All multidate classification overall accuracy results were higher than single date results, with the best multidate result being 8.19 percentage points higher than the best single-date result. For VENuS, there was much less of a difference, with some single-date results outperforming multidate results, and only a 2.22 percentage point difference between the best multidate result and the best single-date result.

4) Planetscope (with four bands and 3 m spatial resolution) outperformed VENuS (11 unique bands, 5 m spatial resolution) for all date combinations. Differences were greatest in urban settings, where different land covers in close proximity resulted in more mixed pixels.

While the results for Planetscope were as expected, VENuS was not greatly improved by the use of multidate imagery. Improving the issues present in this study such as training area selection could yield different results or provide more clarity on the different effects of multitemporal classification for Planetscope and VENuS. Overall, it is clear that with Planetscope combining multiple dates at distinct phenological stages is well suited for distinguishing different types of vegetation.

3.6 References

City of London. 2015. Natural Heritage Inventory and Evaluation, Medway Valley Heritage Forest ESA. https://www.london.ca/residents/Environment/Natural-Environments/Documents/Medway%20NHI-Eval-Final%20Report-Public%20Use-Jan2015.pdf

Drushka, Ken. 2003. Canada's Forests, A History. Montreal: McGill-Queen's University Press.

Harris Geospatial. 2019. "Support Vector Machine".
https://www.harrisgeospatial.com/docs/SupportVectorMachine.html

Hill, R A, A K Wilson, M George, and S A Hinsley. 2010. "Mapping Tree Species in Temperate Deciduous Woodland Using Time-Series Multi-Spectral Data," 86–99. doi:10.1111/j.1654-109X.2009.01053.x.

Jensen, John. 2005. Introductory Digital Image Processing: A Remote Sensing Perspective. 3rd ed. Upper Saddle River, N.J.: Pearson Prentice Hall.

Li, Dan, Yinghai Ke, Huili Gong, and Xiaojuan Li. 2015. "Object-Based Urban Tree Species Classification Using Bi-Temporal Worldview-2 and Worldview-3 Images." Remote Sensing 7 (12): 16917–16937. doi:10.3390/rs71215861.

Lillesand, Thomas M., Ralph W. Kiefer, and Jonathan Chipman. 2008. Remote Sensing and Image Interpretation. 6th ed. John Wiley & Sons.

Louarn, Marine Le, Philippe Clergeau, Elodie Briche, and Magali Deschamps-Cottin. 2017. "'Kill Two Birds with One Stone': Urban Tree Species Classification Using Bi-Temporal Pléiades Images to Study Nesting Preferences of an Invasive Bird." Remote Sensing 9 (9). doi:10.3390/rs9090916.

Pu, Ruiliang. 2017. Hyperspectral Remote Sensing. Boca Raton : Taylor & Francis: CRC Press. doi:10.1201/9781315120607.

Richter, Ronny, Björn Reu, Christian Wirth, Daniel Doktor, and Michael Vohland. 2016. "The Use of Airborne Hyperspectral Data for Tree Species Classification in a Species-Rich Central European Forest Area." International Journal of Applied Earth Observation and Geoinformation 52. Elsevier B.V.: 464–474. doi:10.1016/j.jag.2016.07.018.

Schwartz, Mark D. 2013. "Phenology: An Integrative Environmental Science." Phenology: An Integrative Environmental Science, 1–610. doi:10.1007/978-94-007-6925-0.

Sheeren, David, Mathieu Fauvel, Veliborka Josipović, Maïlys Lopes, Carole Planque, Jérôme Willm, and Jean-François Dejoux. 2016. "Tree Species Classification in Temperate Forests Using Formosat-2 Satellite Image Time Series." Remote Sensing 8 (9): 734. doi:10.3390/rs8090734.

Sozzi, Marco, Francesco Marinello, Andrea Pezzuolo, and Luigi Sartori. 2018. "Benchmark of Satellites Image Services for Precision Agricultural Use." Proceedings of the AgEng Conference, Wageningen, The Netherlands, no. July: 8–11.

Tigges, Jan, Tobia Lakes, and Patrick Hostert. 2013. "Urban Vegetation Classification: Benefits of Multitemporal RapidEye Satellite Data." Remote Sensing of Environment 136: 66–75. doi:10.1016/j.rse.2013.05.001.

Xie, Zhuli, Yaoliang Chen, Dengsheng Lu, Guiying Li, and Erxue Chen. 2019. "Classification of Land Cover, Forest, and Tree Species Classes with ZiYuan-3 Multispectral and Stereo Data." Remote Sensing 11 (2): 164. doi:10.3390/rs11020164.

Zhao, Yuanyuan, Duole Feng, Le Yu, Xiaoyi Wang, Yanlei Chen, Yuqi Bai, H. Jaime Hernández, et al. 2016. "Detailed Dynamic Land Cover Mapping of Chile: Accuracy Improvement by Integrating Multi-Temporal Data." Remote Sensing of Environment 183: 170–185. doi:10.1016/j.rse.2016.05.016.

Chapter 4

4   Conclusion

4.1   Summary

Trees provide numerous benefits to cities, including improving air quality, moderating temperature, improving human health and increasing biodiversity. Many of these services are dependent on the type of tree. Species selection is also important to ensure the survival of the tree depending on the stresses of its location. Finally, many cities consider increasing the number of native species to be a goal. Understanding the species of trees present in a city's urban forest is important, and remote sensing can aid in providing this information through tree classification.

Chapter 2 detailed object-based support vector machine classification of five tree types. Classification features were derived from high-resolution multispectral Geoeye-1 imagery and lidar data. A normalized digital surface model (nDSM) was generated using the lidar point cloud and used to as the basis for marker-controlled watershed segmentation to create tree crown objects. Based on these objects, features were created based on image reflectance, image texture, nDSM texture, lidar height and lidar intensity. Numerous combinations of features were used as input for classification in order to determine which best classify different types of trees.

Chapter 3 tested the ability of multidate Planetscope and VENuS imagery to classify land cover into deciduous trees, coniferous trees, non-tree vegetation and non-vegetation using pixel-based SVM classification. For each sensor, images from April, May, July and October were used individually for classification. Multitemporal classification was then carried out with all four images, and combinations of the July image and one other date.

4.2   Conclusions

The research objectives for both sections of the thesis were completed. The results from chapter 2 were:

1) The best features from high-resolution multispectral imagery and lidar data were identified. GLCM texture measures generated from pansharpened Geoeye-1 imagery were highly useful for classification. The best result from imagery features made use of texture measures of the green and near-infrared bands. GLCM mean was a particularly useful feature. Mean reflectance from imagery did little to increase accuracy when combined with texture measures. For lidar data, intensity metrics were by far the most useful. Middle range (50th and 75th) intensity percentiles were the most useful individual features. The addition of features derived from lidar intensity, lidar height and nDSM texture measures further improved classification accuracy.

2) The combination of features from imagery and lidar data resulted in higher classification accuracy then either could achieve individually. Lidar features outperformed imagery features by 5.88 percentage points. However, the combination of features from both sources of data increased accuracy 7.78 percentage points more than using lidar alone. This resulted in 85.08% overall accuracy when classifying five types of trees.

The conclusions for chapter 3 were:

3) Vegetation classification was improved by using images from multiple seasons. This was most pronounced for Planetscope imagery, where multitemporal classification was 8.19 percentage points higher than the best single-date result. However, the improvement was much lower for VENuS, which only saw a 2.22 percentage point increase. Planetscope outperformed VENuS, achieving 83.11% overall accuracy compared to 72.18% with VENuS.

4) The best dates for differentiating the study's vegetation classes (deciduous trees, coniferous trees, non-tree vegetation) was a combination of April imagery from before leaf growth, with a later image. For Planetscope this was a combination of April and July imagery. Adding May and October images did not further increase overall accuracy. VENuS performed best with May and July imagery, which was slightly more accurate than classification using April and July.

4.3   Contributions

Chapter 2 examined numerous classification features from multispectral imagery and lidar. Although most had been used in previous studies, the various classification tests help to clearly show the capabilities of each feature for classification. For high-resolution multispectral imagery, it was found that the means of grey-level co-occurrence matrix texture measures outperform the mean reflectance of image bands. Therefore, very-high resolution sensors that allow for texture measures of individual trees should make use of them for classification. Lidar data can also provide a source for texture measures through the creation of an nDSM. Using nDSM texture alongside metrics from the lidar point cloud improved accuracy. Relatively few studies make use of texture measures, and when they do their improvement to accuracy is usually not clearly displayed.

Chapter 3 made use of two relatively new sensors, Planetscope and VENuS. As far as I am aware, neither have been used for multitemporal tree classification. For Planetscope, using multiple dates greatly improves its ability to differentiate coniferous and deciduous trees from each other, as well as from other vegetation. The results for VENuS were less clear, with little improvement to accuracy when using multitemporal classification. However as noted in chapter 3, issues may have arisen due to mixed pixels and training area selection. While it is safe to suggest multiple image dates improve tree classification with Planetscope, conclusions are harder to draw for VENuS. Comparing the two sensors, Planetscope outperformed VENuS. While VENuS benefited from a high number of spectral bands, including several in the red edge and near-infrared regions, Planetscope had a higher spatial resolution (5 m compared to 3 m). For classifying urban vegetation, spatial resolution is more significant than spectral resolution as it avoids issues of mixed pixels.

4.4   Discussion

Both sections of the thesis were held back by certain limitations. Chapter 2 was limited by the small number of trees used for classification. While the five chosen tree types were

very common in the study area, many additional species were also present. The results provide useful information on which features distinguish different trees, but they do not demonstrate that the data sources used could allow for even a partial inventory of city trees. This problem is common to most studies on urban tree classification, with only a small number such as Alonzo, Bookhagen, and Roberts 2014 and Zhang and Qiu 2012 classifying a substantial number of species. It could be of interest to attempt a more extensive classification with Geoeye-1 and lidar data, although the relatively low number of species classified in similar studies does not make it seem likely to succeed. However, identifying certain target species still has uses, such as Murfitt et al. 2016 which identified ash trees and assessed their health to monitor the presence of emerald ash borer beetles.

Chapter 3 was limited to a relatively small number of dates. Both VENuS and Planetscope have very frequent revisit times, which should allow for a greater number of dates to be tested. During periods of change to leaves in spring and fall, images only a short time apart may capture different phenological stages. Unfortunately, there is a shortage of imagery in the London area for 2018 and 2019, especially for VENuS. If availability improves, this could allow the strengths of these sensors to better be tested.

4.5   Future Research

The classification scheme in chapter 3 was simple, only distinguishing deciduous and coniferous trees. Individual tree classification seemed infeasible because of the 3 m spatial resolution being coarser than many tree crowns. Kwan et al. 2018 used data fusion methods including STARFM and FSDAF with Planetscope and higher resolution Worldview-2 imagery. This process simulated images with Worlview-2 resolution for dates when only a Planetscope image was available. Worldview-2 and Geoeye-1 both have similar spatial resolution, so simulated images of this pixel size generated from data fusion algorithms using Planetscope and Geoeye-1 could allow for individual tree species classification. Very-high resolution sensors such as Worldview-2 and Geoeye-1 are expensive and have fewer images available, making multitemporal classification difficult. Data fusion with the more accessible Planetscope could allow the power of multitemporal classification to be made use of more easily. However, more research is needed to

determine if fusing these two sensors could create images of sufficient quality for individual tree classification.

4.6   References

Alonzo, M, B Bookhagen, and D A Roberts. 2014. "Urban Tree Species Mapping Using Hyperspectral and Lidar Data Fusion." Remote Sensing of Environment 148 (JANUARY): 70–83. doi:Doi 10.1016/J.Rse.2014.03.018.

Kwan, Chiman, Xiaolin Zhu, Feng Gao, Bryan Chou, Daniel Perez, Jiang Li, Yuzhong Shen, Krzysztof Koperski, and Giovanni Marchisio. 2018. "Assessment of Spatiotemporal Fusion Algorithms for Planet and Worldview Images." Sensors (Switzerland) 18 (4): 1–17. doi:10.3390/s18041051.

Murfitt, Justin, Yuhong He, Jian Yang, Amy Mui, and Kevin De Mille. 2016. "Ash Decline Assessment in Emerald Ash Borer Infested Natural Forests Using High Spatial Resolution Images." Remote Sensing 8 (3): 1–18. doi:10.3390/rs8030256.

Zhang, Caiyun, and Fang Qiu. 2012. "Mapping Individual Tree Species in an Urban Forest Using Airborne Lidar Data and Hyperspectral Imagery." Photogrammetric Engineering & Remote Sensing 78 (10): 1079–1087. doi:10.14358/PERS.78.10.1079.

Appendices

Appendix A: Classification features used in chapter 2

Table A-1 Metrics generated using zonal statistics in ArcGIS

Feature Name	Description
Mean	Mean of pixels within object
Standard Deviation	Standard deviation of pixels within object

Table A-2 Texture measures generated using TEX in PCI Geomatica, for pansharpened Geoeye bands, shaded relief, and nDSM

Feature Name	Equation	Description
Angular 2nd Moment	`SUM(i,j=0,N-1)(P(i,j)**2)`	Measure of orderliness of image, higher value is more orderly
Contrast	`SUM(i,j=0,N-1)(P(i,j)*(i-j)**2)`	Measure of difference between pixel values of neighbouring pixels
Correlation	`SUM(i,j=0,N-1)(P(i,j)*(i-Mean_i)*(j-Mean_j))/SQRT(Var_i * Var_j)`	Measures predictability of relationship between neighbouring pixel values
Dissimilarity	`SUM(i,j=0,N-1)(P(i,j)*|i-j|)`	Similar to contrast, measure of difference between pixel values
Entropy	`SUM(i,j=0,N-1)(-P(i,j) * LOGe(P(i,j))),  assuming that 0 * LOGe(0) = 0.`	Measure of orderliness, higher value in less orderly
Homogeneity	`SUM(i,j=0,N-1)(P(i,j)/(1+(i-j)**2))`	Measure of the similarity of pixel values of neighbouring pixels
Mean	`SUM(i,j=0,N-1)(i*P(i,j))`	Mean based on GLCM matrix (rather than simply means in image)

Standard Deviation	`Var_i = SUM(i,j=0,N-1)(P(i,j)*(i - Mean_i)**2)`
	
	`Std. Deviation_i = SQRT(Var_i)`
	
	Top equation is variance, standard deviation is square root of variance
		Standard deviation based on GLCM matrix

GLDV Angular 2nd Moment	`SUM(k=0,N-1)(V(k)**2)`	Measure of orderliness, based on GLDV derived from GLCM matrix
GLDV Contrast	`SUM(k=0,N-1)(V(k) * k**2)`	Contrast measure based on GLDV
GLDV Entropy	`SUM(k=0,N-1)(-V(k)*LOGe(V(k)), assuming that 0*LOGe(0)= 0`	Entropy measure based on GLDV
GLDV Mean	`SUM(k=0,N-1)(V(k)*k)`	Mean based on GLDV

Table A-3 Lidar height metrics generated using LASCanopy

All these metrics are based on the lidar points higher than 1.37 m found within the area of a tree crown object.

Feature Name	Description
Height Minimum	Lowest height value
Height Maximum	Highest height values
Height Mean	Mean height value
Height Average Square Value	Square root of mean of squared height values
Height Standard Deviation	Standard deviation of height values
Height Skewness	Represents to what degree height values are more often higher or lower than the mean
Height Kurtosis	Represents the shape of the distribution of height points, to what degree they diverge from the mean
Height Percentiles	The height value that N% of lidar points fall below. (e.g. 10th percentile is the height value that 10% of lidar points fall below). This is normalized to percent of a tree's height (e.g. if tree is 20 m, and 90th percentile value is 16 m, the value is normalized to 0.8)

Table A-4 Lidar intensity metrics generated using LASCanopy

Intensity Minimum	Lowest intensity value
Intensity Maximum	Highest intensity values
Intensity Mean	Mean intensity value
Intensity Average Square Value	Square root of mean of squared intensity values
Intensity Standard Deviation	Standard deviation of intensity values
Intensity Skewness	Represents to what degree intensity values are more often higher or lower than the mean
Intensity Kurtosis	Represents the shape of the distribution of intensity points, to what degree they diverge from the mean
Intensity Percentiles	The intensity value that N% of lidar points fall below. (e.g. 10th percentile is the intensity value that 10% of lidar points fall below). This is not normalized.

Appendix B: Confusion matrices for chapter 2

Table B-1 Confusion matrix of the classification using Geoeye reflectance Features

	Norway maple	Schwedleri Norway maple	Honey locust	Colorado blue spruce	Littleleaf linden	Total
Norway maple	56	12	12	8	11	**99**
Schwedleri Norway maple	8	57	1	2	2	**70**
Honey locust	12	2	48	16	12	**90**
Colorado blue spruce	5	1	11	51	14	**82**
Littleleaf linden	11	10	20	9	57	**107**
Total	**92**	**82**	**92**	**86**	**96**	

Table B-2 Confusion matrix of the classification using Geoeye texture features

	Norway maple	Schwedleri Norway maple	Honey locust	Colorado blue spruce	Littleleaf linden	Total
Norway maple	66	17	10	7	6	**106**
Schwedleri Norway maple	14	55	2	2	12	**85**
Honey locust	4	2	62	1	4	**73**
Colorado blue spruce	1	0	2	71	7	**81**
Littleleaf linden	7	8	16	5	67	**103**
Total	**92**	**82**	**92**	**86**	**96**	

Table B-3 Confusion matrix of the classification using Shaded Relief texture features

	Norway maple	Schwedleri Norway maple	Honey locust	Colorado blue spruce	Littleleaf linden	Total
Norway maple	48	28	12	3	10	**101**
Schwedleri Norway maple	16	22	7	1	8	**54**
Honey locust	16	20	72	1	5	**114**
Colorado blue spruce	4	6	0	62	16	**88**
Littleleaf linden	8	6	1	19	57	**91**
Total	**92**	**82**	**92**	**86**	**96**	

Table B-4 Confusion matrix of the classification using nDSM Texture features

	Norway maple	Schwedleri Norway maple	Honey locust	Colorado blue spruce	Littleleaf linden	Total
Norway maple	51	21	15	1	8	**96**
Schwedleri Norway maple	5	17	17	1	14	**54**
Honey locust	23	33	53	1	4	**114**
Colorado blue spruce	3	2	3	77	14	**99**
Littleleaf linden	10	9	4	6	56	**85**
Total	**92**	**82**	**92**	**86**	**96**	

Table B-5 Confusion matrix of the classification using lidar height features

	Norway maple	Schwedleri Norway maple	Honey locust	Colorado blue spruce	Littleleaf linden	Total
Norway maple	48	23	31	2	14	**118**
Schwedleri Norway maple	12	16	12	5	11	**56**
Honey locust	18	17	37	1	10	**83**
Colorado blue spruce	3	11	2	69	14	**99**
Littleleaf linden	11	15	10	9	47	**92**
Total	**92**	**82**	**92**	**86**	**96**	

Table B-6 Confusion matrix of the classification using lidar intensity features

	Norway maple	Schwedleri Norway maple	Honey locust	Colorado blue spruce	Littleleaf linden	Total
Norway maple	41	17	0	7	1	**66**
Schwedleri Norway maple	25	54	0	0	15	**94**
Honey locust	5	0	74	0	16	**95**
Colorado blue spruce	16	2	1	79	1	**99**
Littleleaf linden	5	9	17	0	63	**94**
Total	**92**	**82**	**92**	**86**	**96**	

Table B-7 Confusion matrix of the classification using combined Geoeye and Lidar Features (Best Result)

	Norway maple	Schwedleri Norway maple	Honey locust	Colorado blue spruce	Littleleaf linden	Total
Norway maple	71	19	2	2	2	**96**
Schwedleri Norway maple	13	56	2	0	5	**76**
Honey locust	4	3	86	0	5	**98**
Colorado blue spruce	1	0	0	84	0	**85**
Littleleaf linden	3	4	2	0	84	**93**
Total	**92**	**82**	**92**	**86**	**96**	

Appendix C: Confusion matrices for chapter 3

Table C-1 Confusion matrix of the classification for Planet Four-date

	Deciduous	Conifer	Other Vegetation	Non- Vegetation	Total
Deciduous	126	5	15	2	**148**
Conifer	10	22	3	1	**36**
Other Vegetation	30	3	128	18	**179**
Non-Vegetation	3	0	9	211	**223**
Total	**169**	**30**	**155**	**232**	

Table C-2 Confusion matrix of the classification for Planet April

	Deciduous	Conifer	Other Vegetation	Non-Vegetation	Total
Deciduous	107	7	10	15	**139**
Conifer	11	18	2	0	**31**
Other Vegetation	30	5	88	35	**158**
Non-Vegetation	21	0	11	226	**258**
Total	**169**	**30**	**111**	**276**	

Table C-3 Confusion matrix of the classification for Planet May

	Deciduous	Conifer	Other Vegetation	Non-Vegetation	Total
Deciduous	97	13	10	9	**129**
Conifer	19	13	3	0	**35**
Other Vegetation	37	4	97	47	**185**
Non-Vegetation	16	0	9	212	**237**
Total	**169**	**30**	**119**	**268**	

Table C-4 Confusion matrix of the classification for Planet July

	Deciduous	Conifer	Other Vegetation	Non-Vegetation	Total
Deciduous	34	0	2	0	**36**
Conifer	51	16	13	4	**84**
Other Vegetation	77	14	115	11	**217**
Non-Vegetation	7	0	14	228	**249**
Total	**169**	**30**	**144**	**243**	

Table C-5 Confusion matrix of the classification for Planet October

	Deciduous	Conifer	Other Vegetation	Non-Vegetation	Total
Deciduous	65	14	8	11	**98**
Conifer	41	13	5	3	**62**
Other Vegetation	44	3	87	24	**158**
Non-Vegetation	19	0	14	235	**268**
Total	**169**	**30**	**114**	**273**	

Table C-6 Confusion matrix of the classification for Planet April/July

	Deciduous	Conifer	Other Vegetation	Non-Vegetation	Total
Deciduous	125	5	14	3	**147**
Conifer	9	20	4	1	**34**
Other Vegetation	29	5	129	17	**180**
Non-Vegetation	6	0	6	213	**225**
Total	**169**	**30**	**153**	**234**	

Table C-7 Confusion matrix of the classification for Planet May/July

	Deciduous	Conifer	Other Vegetation	Non-Vegetation	Total
Deciduous	117	7	11	2	**137**
Conifer	19	18	6	2	**45**
Other Vegetation	29	5	135	23	**192**
Non-Vegetation	4	0	2	206	**212**
Total	**169**	**30**	**154**	**233**	

Table C-8 Confusion matrix of the classification for Planet October/July

	Deciduous	Conifer	Other Vegetation	Non-Vegetation	Total
Deciduous	96	4	8	1	**109**
Conifer	37	18	5	2	**62**
Other Vegetation	32	8	131	10	**181**
Non-Vegetation	4	0	9	221	**234**
Total	**169**	**30**	**153**	**234**	

Table C-9 Confusion matrix of the classification for VENuS Four-date

	Deciduous	Conifer	Other Vegetation	Non-Vegetation	Total
Deciduous	112	8	23	3	**146**
Conifer	14	13	3	4	**34**
Other Vegetation	32	8	118	48	**206**
Non-Vegetation	10	1	16	173	**200**
Total	**168**	**30**	**160**	**228**	

Table C-10 Confusion matrix of the classification for VENuS April

	Deciduous	Conifer	Other Vegetation	Non-Vegetation	Total
Deciduous	90	7	5	7	**109**
Conifer	10	15	6	0	**31**
Other Vegetation	41	7	91	47	**186**
Non-Vegetation	27	1	14	218	**260**
Total	**168**	**30**	**116**	**272**	

Table C-11 Confusion matrix of the classification for VENuS May

	Deciduous	Conifer	Other Vegetation	Non-Vegetation	Total
Deciduous	87	6	8	7	**108**
Conifer	6	12	3	3	**24**
Other Vegetation	49	10	95	41	**195**
Non-Vegetation	26	2	15	216	**259**
Total	**168**	**30**	**121**	**267**	

Table C-12 Confusion matrix of the classification for VENuS July

	Deciduous	Conifer	Other Vegetation	Non-Vegetation	Total
Deciduous	57	5	9	3	**74**
Conifer	64	16	12	8	**100**
Other Vegetation	43	8	113	55	**219**
Non-Vegetation	4	1	15	173	**193**
Total	**168**	**30**	**149**	**239**	

Table C-13 Confusion matrix of the classification for VENuS October

	Deciduous	Conifer	Other Vegetation	Non-Vegetation	Total
Deciduous	70	5	12	1	**88**
Conifer	39	15	7	6	**67**
Other Vegetation	43	7	84	34	**168**
Non-Vegetation	16	3	17	227	**263**
Total	**168**	**30**	**120**	**268**	

Table C-14 Confusion matrix of the classification for VENuS April/July

	Deciduous	Conifer	Other Vegetation	Non-Vegetation	Total
Deciduous	113	5	12	3	**133**
Conifer	15	16	7	3	**41**
Other Vegetation	30	8	125	58	**221**
Non-Vegetation	10	1	13	167	**191**
Total	**168**	**30**	**157**	**231**	

Table C-15 Confusion matrix of the classification for VENuS May/July

	Deciduous	Conifer	Other Vegetation	Non-Vegetation	Total
Deciduous	103	4	13	5	**125**
Conifer	19	14	4	4	**41**
Other Vegetation	39	11	131	46	**227**
Non-Vegetation	7	1	10	175	**193**
Total	**168**	**30**	**158**	**230**	

Table C-16 Confusion matrix of the classification for VENuS October/July

	Deciduous	Conifer	Other Vegetation	Non-Vegetation	Total
Deciduous	82	5	11	4	**102**
Conifer	45	19	6	6	**76**
Other Vegetation	35	5	129	45	**214**
Non-Vegetation	6	1	11	176	**194**
Total	**168**	**30**	**157**	**231**	

Appendix D: Classification maps for chapter 3

Figure D-1
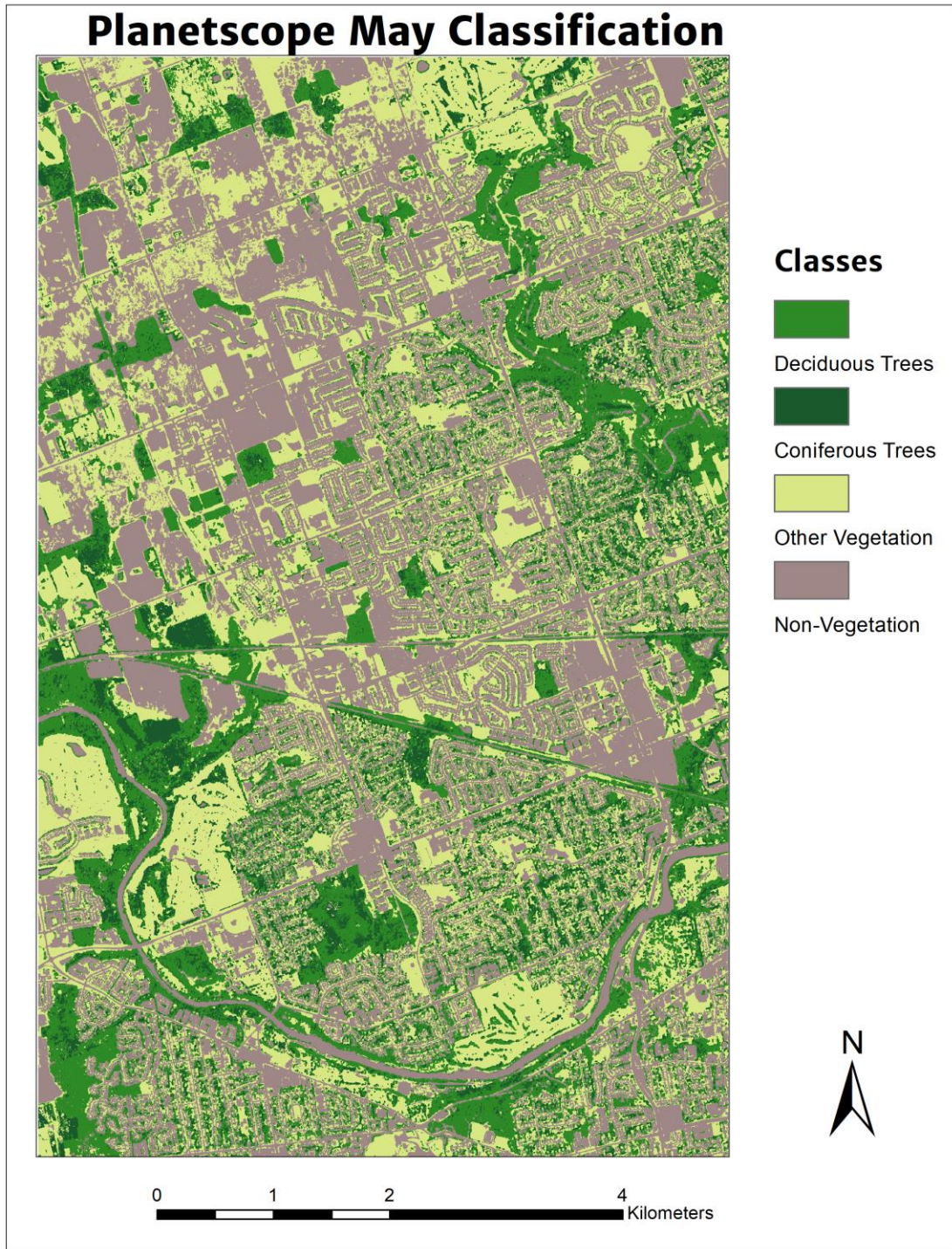
Figure D-2

Figure D-3

Figure D-4

Planetscope April/July Classification

Classes

Deciduous Trees

Coniferous Trees

Other Vegetation

Non-Vegetation

0   1   2   4
Kilometers

N

Figure D-5

Figure D-6

Figure D-7

Figure D-8

Figure D-9

Figure D-10

Figure D-11

Figure D-12

Figure D-13

Figure D-14

Curriculum Vitae

Name:　　　　　Matthew Roffey

Post-secondary　The University of Western Ontario
Education and　London, Ontario, Canada
Degrees:　　　　2011-2015 B.A.

　　　　　　　　　The University of Western Ontario
　　　　　　　　　London, Ontario, Canada
　　　　　　　　　2017-2019 M.Sc.

Honours and　　Ontario Graduate Scholarship
Awards:　　　　2017-2018

Related Work　　Teaching Assistant
Experience　　　The University of Western Ontario
　　　　　　　　　2017-2019

Conferences: Roffey, M. and Wang, J., 2019. "Classification of urban tree species using high-resolution multispectral imagery and LiDAR in London, Ontario", presented at 40th Canadian Symposium on Remote Sensing & Geomatics, June 4-6th.